NASA Contractor Report 3480

Feasibility Study of a Procedure To Detect and Warn of Low-Level Wind Shear

Barry S. Turkel, Philip A. Kessel,
and Walter Frost

CONTRACT NAS8-33458
NOVEMBER 1981

NASA

NASA Contractor Report 3480

Feasibility Study of a Procedure To Detect and Warn of Low-Level Wind Shear

Barry S. Turkel, Philip A. Kessel,
and Walter Frost
FWG Associates, Inc.
Tullahoma, Tennessee

Prepared for
George C. Marshall Space Flight Center
under Contract NAS8-33458

National Aeronautics
and Space Administration

**Scientific and Technical
Information Branch**

1981

ACKNOWLEDGMENTS

The authors are grateful to A. Richard Tobiason for the support of NASA under Contract NAS8-33458. Technical inputs provided by Mr. Dennis Camp, NASA Marshall Space Flight Center, Atmospheric Sciences Division, Huntsville, Alabama, and Dr. John McCarthy, National Center for Atmospheric Research, Boulder, Colorado, are also gratefully acknowledged. The authors also wish to thank Richard Bray of NASA Ames Research Center, Moffett Field, California, for his cooperation and technical assistance during the flight simulator tests.

TABLE OF CONTENTS

CHAPTER		PAGE
1	INTRODUCTION	1
2	AIRCRAFT TRAJECTORY PROGRAM	6
	2.1 Program Specifics	6
	2.2 Equations of Motion	7
	2.3 Pilot/Control System Models	9
3	FLIGHT PATH DETERIORATION PARAMETERS	15
4	RESULTS OF COMPUTER AND SIMULATOR STUDIES	18
	4.1 Description of Test Plan	18
	4.2 Illustration of Aircraft Sensitivity to Longitudinal Wind Shears at Various Frequencies	18
	4.3 Computed Aircraft Trajectory Results	26
	4.3.1 Sine Waves	26
	4.3.2 1 - Cosine Downbursts	33
	4.3.3 S-Shape Waves	38
	4.3.4 Combination S-Shape Waves and Downbursts	41
5	DESCRIPTION OF FLIGHT SIMULATOR TESTS CONDUCTED AT NASA AMES	51
	5.1 Flight Simulator Results	51
	5.1.1 Sine Waves (Figures 9 and 11)	51
	5.1.2 1 - Cosine Downbursts (Figures 13 and 15)	52
	5.1.3 S-Shape Waves (Figures 17 and 19)	53
	5.1.4 Combination S-Shape Waves and Downbursts (Figure 23)	54

CHAPTER PAGE

5.2 Comparisons Between Computer Results and Simulator Results 55

6 CONCLUDING REMARKS 62

APPENDIX A: LANDING CHARACTERISTICS OF A B727 CLASS MEDIUM-SIZED JET TRANSPORT 66

APPENDIX B: SAMPLE CALCULATION OF FLIGHT PATH DETERIORATION PARAMETERS 67

LIST OF ILLUSTRATIONS

FIGURE	TITLE	PAGE
1	Doppler Radar Linked to Microprocessor	3
2	Doppler Radar Wind Shear Warning and Detection System	4
3	Relationship Between the Various Forces Acting on an Aircraft	8
4	Concept of Flight Path Deterioration Parameters (FPDP)	16
5	Wind Models Used to Simulate a Thunderstorm Downburst Cell	19
6	Computer-Simulated Approach Trajectory of a B727 with Fixed Controls Through a Longitudinal Sine Wave Wind	23
7	Computer-Simulated Approach Trajectory of a B727 Using Control System I Through a Longitudinal Sine Wave Wind	25
8	Computer-Simulated Approach Trajectory of a B727 Using Control System II Through a Longitudinal Sine Wave Wind	27
9	Approach Trajectory of a B727 Aircraft Performed by a Test Pilot in the NASA Ames Simulator Through a Longitudinal Sine Wave Wind	28
10	Computer-Simulated Approach Trajectory of a B727 Using Control System II Through a Longitudinal Sine Wave Wind	30
11	Approach Trajectory of a B727 Aircraft Performed by a Test Pilot in the NASA Ames Simulator Through a Longitudinal Sine Wave Wind	31
12	Computer-Simulated Approach Trajectory of a B727 Using Control System II Through a Vertical 1 - Cosine Wave Downburst	34
13	Approach Trajectory of a B727 Aircraft Performed by a Test Pilot in the NASA Ames Simulator Through a Vertical 1 - Cosine Wave Downburst	35
14	Computer-Simulated Approach Trajectory of a B727 Using Control System II Through a Vertical 1 - Cosine Wave Downburst	36

FIGURE	TITLE	PAGE
15	Approach Trajectory of a B727 Aircraft Performed by a Test Pilot in the NASA Ames Simulator Through a Vertical 1 - Cosine Wave Wind	37
16	Computer-Simulated Approach Trajectory of a B727 Using Control System II Through a Longitudinal S-Shape Wave Wind	39
17	Approach Trajectory of a B727 Aircraft Performed by a Test Pilot in the NASA Ames Simulator Through a Longitudinal S-Shape Wave Wind	40
18	Computer-Simulated Approach Trajectory of a B727 Using Control System II Through a Longitudinal S-Shape Wave Wind	42
19	Approach Trajectory of a B727 Aircraft Performed by a Test Pilot in the NASA Ames Simulator Through a Longitudinal S-Shape Wave Wind	43
20	The Flight Path of Eastern 66 and Associated Wind Field as Analyzed by Fujita and Caracena [2]	44
21	Computer-Simulated Approach Trajectory of a B727 Using Control System II Through a Combination Longitudinal S-Shape and Vertical 1 - Cosine Wave Wind	46
22	Computer-Simulated Approach Trajectory of a B727 Using Control System II Through a Combination Longitudinal S-Shape and Vertical 1 - Cosine Wave Wind	47
23	Approach Trajectory of a B727 Aircraft Performed by a Test Pilot in the NASA Ames Simulator Through a Combination Longitudinal S-Shape and Vertical 1 - Cosine Wave Wind	48
24	Computer-Simulated Approach Trajectory of a B727 Using Control System III Through a Longitudinal Sine Wave Wind of 15.45 m/s Amplitude and ω_{ph} Frequency	50
25	Airspeed Deviation Parameters for Longitudinal Sine Wave Winds	57
26	Airspeed Deviation Parameters for Longitudinal S-Shape Wave Winds	58
27	Airspeed Deviation Parameters for Vertical 1 - Cosine Wave Winds	60
28	Airspeed Deviation Parameters for Combination Longitudinal S-Shape and Vertical 1 - Cosine Wave Winds	61

LIST OF TABLES

TABLE	TITLE	PAGE
1	Test Plan for Simulator and Computer Runs	20
2	Flight Trajectory Computer Run Summary	21
3	Flight Trajectory Simulator Run Summary	22

DEFINITION OF SYMBOLS

SYMBOL	DEFINITION
A	Aircraft reference wing area (m^2)
C_D	Drag coefficient, $D/(1/2)\rho V^2 A$ (dimensionless)
C_{D_o}	Drag coefficient at zero angle of attack (dimensionless)
C_{D_α}	Drag derivative (rad^{-1})
$C_{D_{\alpha^2}}$	Drag derivative (rad^{-2})
$C_{D_{\delta_E}}$	Drag derivative (rad^{-1})
C_L	Lift coefficient $L/(1/2)\ \rho V^2 A$ (dimensionless)
C_{L_o}	Lift coefficient at zero angle of attack (dimensionless)
C_{L_q}	Lift derivative (rad^{-1})
C_{L_α}	Lift derivative (rad^{-1})
$C_{L_{\dot{\alpha}}}$	Lift derivative (rad^{-1})
$C_{L_{\delta_E}}$	Lift derivative (rad^{-1})
C_m	Pitching-moment coefficient $M/(1/2)\rho V^2 A\bar{c}$ (dimensionless)
C_{m_o}	Pitching-moment coefficient at zero angle of attack (dimensionless)
C_{m_q}	Pitching-moment derivative (rad^{-1})
C_{m_α}	Pitching-moment derivative (rad^{-1})
$C_{m_{\dot{\alpha}}}$	Pitching-moment derivative (rad^{-1})
$C_{m_{\delta E}}$	Pitching-moment derivative (rad^{-1})
$\bar{c}$	Wing mean aerodynamic chord (m)
D	Aerodynamic drag force (N)

SYMBOL	DEFINITION
F	Net propulsive thrust (N)
g	Acceleration due to gravity (m/s^2)
GS+	Flight path deterioration parameter for ascent above glide slope (dimensionless)
GS-	Flight path deterioration parameter for descent below glide slope (dimensionless)
I_{yy}	Aircraft moment of inertia about lateral y axis ($kg - m^2$)
L	Aerodynamic lift force (N)
m	Aircraft mass (kg)
M	Pitching moment ($kg\ m^2/s^2$)
q	Pitch angular velocity (rad/sec)
t_c	Engine characteristic spool-up time (sec)
V	Magnitude of airspeed (m/s)
V_{ref}	Magnitude of initial airspeed (m/s)
V+	Flight path deterioration parameter for airspeed deviation above V_{ref} (m/s)
V-	Flight path deterioration parameter for airspeed deviation below V_{ref} (m/s)
W_x	Magnitude of horizontal wind component (head wind +, tail wind -) (m/s)
W_z	Magnitude of vertical wind component (down draft +, updraft -) (m/s)
x	Horizontal coordinate (m)
$\dot{x}$	Aircraft ground speed (m/s)
z	Vertical coordinate (m)
$\dot{z}$	Aircraft vertical velocity (m/s)

Greek Symbols

α	Aircraft angle of attack (rad)

SYMBOL	DEFINITION
δ_E	Elevator deflection angle (rad)
Δ	Denotes differential
θ	Aircraft pitch angle (rad)
ρ	Air density (kg/m^3)
ω_{ph}	Phugoid frequency (sec^{-1})

Other

$(\dot{})$	First time derivative
$(\ddot{})$	Second time derivative
$(\ )_N$	Nominal (trim) value
$(\ )_o$	Initial value

CHAPTER 1. INTRODUCTION

Several aircraft accidents and near accidents have been officially attributed to encounter with low-level wind shear during the approach and takeoff phases of operation. The most notable accident with wind shear as a major cause involved the Eastern 66 Boeing 727 (B727) which crashed on approach in a thunderstorm wind environment at John F. Kennedy (JFK) International Airport on June 24, 1975, resulting in 113 fatalities [1].*

Wind shear is a spatial or temporal gradient in wind speed and/or direction. Strong shears are generally associated with the presence of cold and warm fronts and thunderstorm cells. An analysis of the Eastern 66 accident by Fujita and Caracena [2] revealed that Eastern 66 was forced above and then subsequently below the glide slope when it flew directly into a downburst cell consisting of a strong down draft and a head wind shearing to a tail wind.

While Fujita blamed the accident on the presence of strong down drafts, several subsequent studies by McCarthy, Blick, and Bensch [3], Frost and Crosby [4], Frost and Reddy [5], and Turkel and Frost [6] focused mainly on fixed-controlled and pilot-controlled aircraft response to longitudinal wind shears, which excite the aircraft's phugoidal (long period) oscillatory mode. The phugoidal time period, which depends on the aircraft's airspeed (approximately 70 m/s for a B727 on approach), is about 38 sec. At an approach ground speed of 70 m/s, an aircraft flies 2.7 km in 38 sec. This is well within a thunderstorm downburst cell's horizontal extent [2]. It is therefore possible for an aircraft on approach to encounter a thunderstorm downburst cell and experience a wave-like head wind to tail wind shear at approximately the aircraft's phugoidal frequency. During the thunderstorm at JFK, several aircraft

---

*Numbers in brackets correspond to similarly numbered references in the list of references.

landed with varying degrees of success. Seven aircraft experienced little or no problem; one had extreme difficulty; one executed a missed approach; and Eastern 66 crashed. Fujita theorized that these aircraft passed through various sections of several downburst centers crossing the approach path at various times and that Eastern 66 flew directly into the center of a strong cell.

Since the accident, several wind shear detection and warning systems and operational procedures have been proposed to prevent further accidents and alert flight crews and air traffic controllers to the presence of wind shear. Examples include LLWSAS (low level wind shear alert system) [7], PJDS (pressure jump detector system) [8], and the airspeed-ground speed operational procedure [7]. However, none of the proposed systems provides a warning of severe wind shear located along the approach path prior to encounter by the aircraft. The LLWSAS and PJDS provide low level warning at the ground at the airport and in its surrounding areas. The airspeed-ground speed monitoring procedure requires the aircraft to be already in the wind shear and to have ground speed information readily available.

A wind shear warning and detection system capable of providing adequate warning of severe wind shear has been proposed by McCarthy [9]. The system would consist of a Doppler radar, a microprocessor, a data link, and displays. The Doppler radar (Figure 1) would be located near the runway, aimed along the approach or takeoff path, and would be programmed to rapidly measure horizontal wind components at 150 m slant length intervals between the ground and an altitude of 500 m. The measured flight path longitudinal wind field and the aircraft configuration designation would be entered into a microprocessor which would then integrate the equations of motion to predict the aircraft's probable deviation from its desired flight path and to compute a set of parameters which describe the aircraft's deviation from its desired flight path. These so-called flight path deterioration parameters, which will be discussed in detail below, are used to quantify the aircraft's trajectory behavior as a single set of numbers. The flight path deterioration parameters would then be transmitted via the data link to the air traffic controller and pilot's data display (Figure 2).

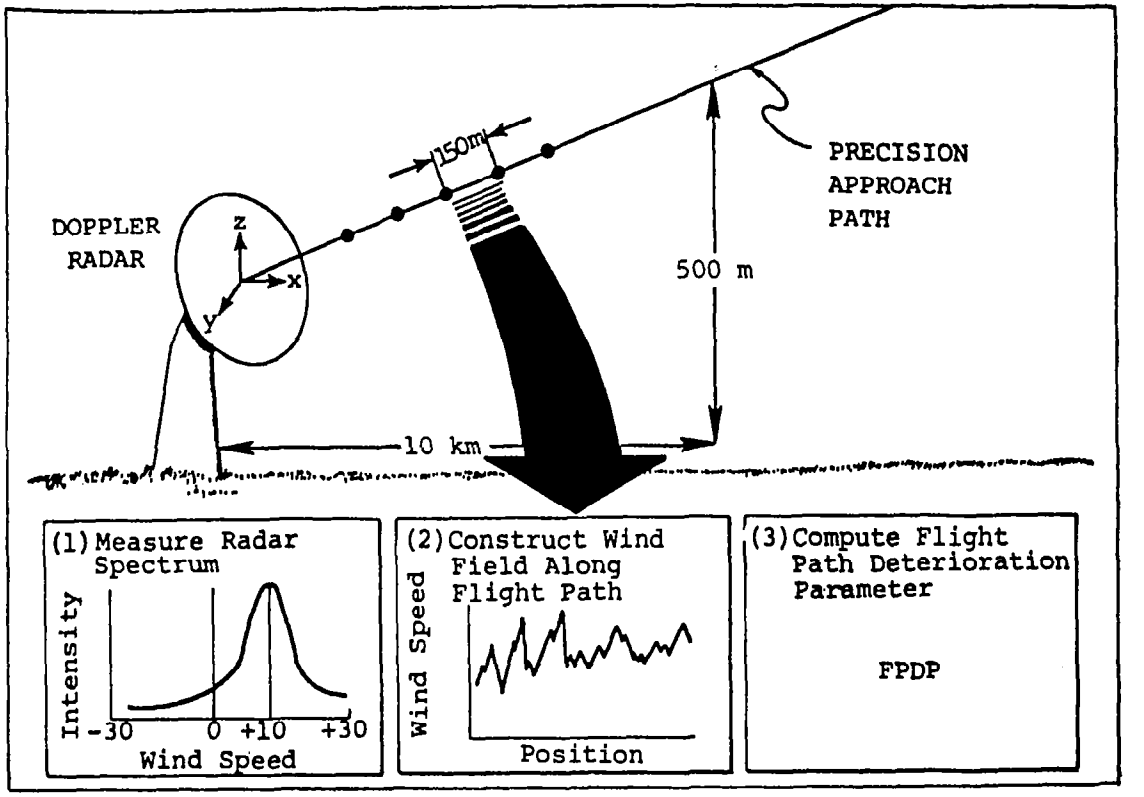

Figure 1 Doppler radar linked to microprocessor.

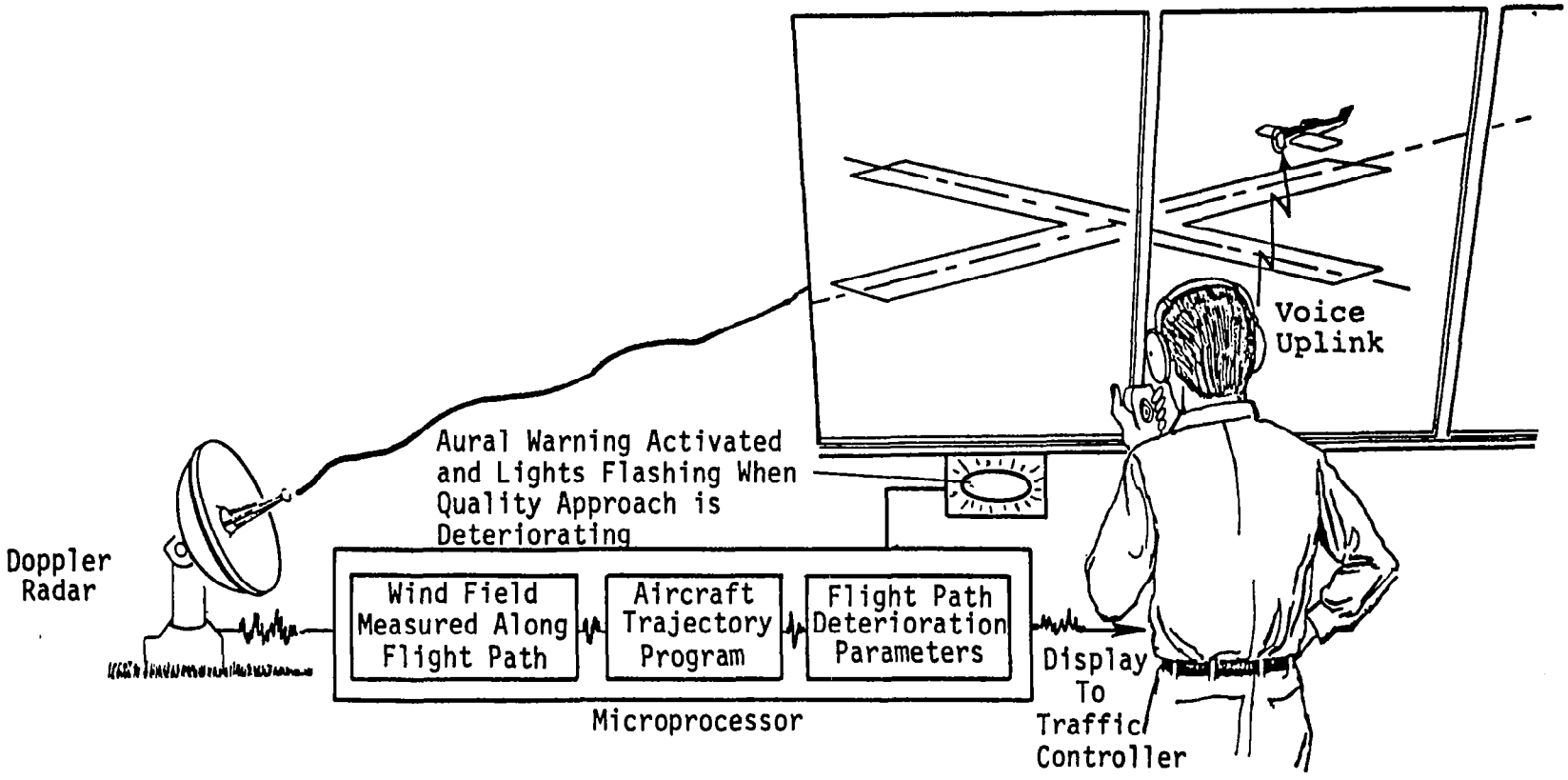

Figure 2 Doppler radar wind shear warning and detection system.

The Doppler radar is an excellent device for wind speed detection since it can measure the longitudinal wind for long distances along flight paths. One Doppler beamed along the glide slope only measures the wind velocity component that is aligned with the Doppler beam, which is approximately equal to the horizontal wind component along the flight path. Because the vertical velocities along the glide slope are difficult to measure with Doppler radar and because the longitudinal winds directly affect the aircraft's longitudinal stability, attention is focused on using only longitudinal wind data as input to warning system software. The vertical velocity components should not be ignored, however, since they clearly influence the longitudinal wind field.

The aim of this study is:

1. To utilize an aircraft trajectory program to examine aircraft/pilot response through wind shears including longitudinal sine waves, S-shape waves, 1 - cosine vertical winds, and combinations at various frequencies and amplitudes as approximations to the winds encountered in a thunderstorm downburst cell.

2. To determine if the control system algorithm and aircraft trajectory program combination gives an accurate representation of the behavior of the real pilot in a flight simulator and hence real aircraft when subjected to the input wind field models described above.

This report will discuss the trajectory program, the pilot/control system models, the quantitative flight path deterioration parameters, the trajectory program results, the flight simulator results, and will present conclusions and recommendations.

CHAPTER 2. AIRCRAFT TRAJECTORY PROGRAM

2.1 Program Specifics

The aircraft trajectory program is a two-dimensional, three-degree-of-freedom model with translational motion in the longitudinal (x) and vertical (z) planes and rotational motion about the lateral (y) axis. A two-dimensional model is sufficient for a warning and detection system since we are looking primarily at the effects of longitudinal winds along the glide slope which cause the aircraft deviations in the x-z plane of the glide slope. The effects of lateral winds on the aircraft's horizontal deviation of the glide slope have not been included in the aircraft trajectory model since the lateral wind component cannot be measured by the single Doppler radar. The three-degree-of-freedom warning system program developed in this study requires little computer storage capacity and has execution times compatible with real-time field operations. It should be noted that the aircraft trajectory program was derived from the previous model of Turkel and Frost [6]. The program was compacted and the pilot/control system was both improved and simplified. The new model has a run time less than 3 sec on a VAX 11/780 as compared to 50 sec for the previous model. The equations of motion are discussed in Section 2.2.

The aircraft trajectory program is adaptable to any aircraft. The aerodynamic lift, drag, and moment coefficients and other data (i.e., wing area, weight) and the initial control settings must be input by the user. In a real-time system, these data may be stored by aircraft type to be looked up for a specific aircraft entering the warning zone. In addition, the program can be run in the takeoff or landing configuration. The Doppler-measured longitudinal winds can be entered as a function of horizontal distance from the runway threshold in a subroutine to be utilized in the simulation of the aircraft's trajectory. After the simulated trajectory through the Doppler-monitored warning zone is completed,

the flight path deterioration parameters based on airspeed and flight path deviation can be calculated and any potential hazards due to the longitudinal wind field can be identified by the air traffic controller. These parameters are described in Chapter 3.

The trajectory program control systems can simulate aircraft control by autopilots or pilots of varying degrees of skill. Engine spool-up lag and pilot thrust command delay are included. These thrust command lags due to the pilot response delay and the turbomachinery response characteristics are important factors in a longitudinal wind shear encounter where the aircraft needs a large power increase in a short time to stay out of danger. The control systems are described in detail in Section 2.3.

2.2 Equations of Motion

The forces acting on the aircraft and angular relationships for the two-dimensional, three-degree-of-freedom model are presented in Figure 3. The equations of motion in earth coordinates are:

1) Acceleration along longitudinal axis

$$\ddot{x} = \frac{F}{m} \cos \theta - \frac{L}{m} \sin(\gamma) - \frac{D}{m} \cos(\gamma) \tag{1}$$

2) Acceleration along vertical axis

$$\ddot{z} = \frac{F}{m} \sin \theta + \frac{L}{m} \cos(\gamma) - \frac{D}{m} \sin(\gamma) - g \tag{2}$$

3) Acceleration about lateral axis

$$\ddot{\theta} = \frac{M}{I_{yy}} \tag{3}$$

where aircraft lift, drag, and moment are given respectively by

$$L = 1/2 \, \rho V^2 C_L A \tag{4}$$

$$D = 1/2 \, \rho V^2 C_D A \tag{5}$$

$$M = 1/2 \, \rho V^2 C_m A \bar{c} \tag{6}$$

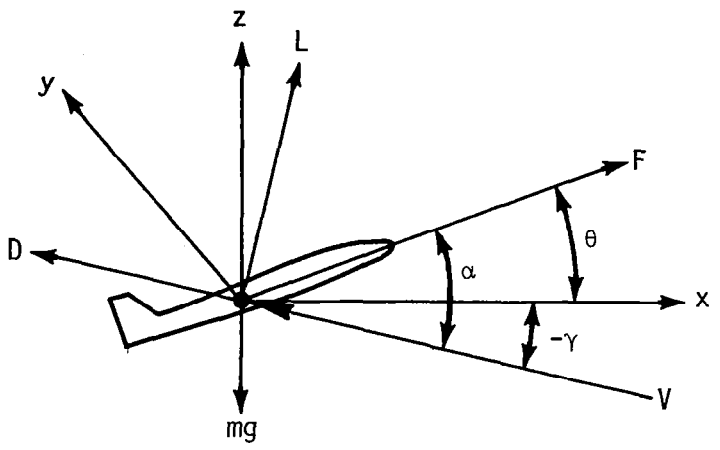

Figure 3 Relationship between the various forces acting on an aircraft.

The magnitude of the relative wind vector, i.e., the airspeed, is given by

$$V = [(\dot{x} + W_x)^2 + (\dot{z} + W_z)^2]^{1/2} \tag{7}$$

where $\dot{x}$ and $\dot{z}$ are the aircraft ground speed and vertical velocity relative to the earth. W_x is the longitudinal wind speed component and is defined as positive when opposing the aircraft and is hence called the head wind. Similarly, W_z is the vertical wind speed component and is defined as positive in the negative z direction and is commonly called the down draft.

The angle γ is given by

$$\gamma = \tan^{-1}\left(\frac{\dot{z} + W_z}{\dot{x} + W_x}\right) \tag{8}$$

and angle of attack is given by

$$\alpha = \theta + (-\gamma) = \theta - \gamma \tag{9}$$

The aerodynamic lift, drag, and moment coefficients in Equations 4 through 6 are given by

$$C_L = C_{L_o} + C_{L_\alpha}(\alpha) + C_{L_{\delta_E}}(\delta_E) + \frac{\bar{c}}{2V} C_{L_q}(q) + \frac{\bar{c}}{2V} C_{L_{\dot{\alpha}}}(\dot{\alpha}) \tag{10}$$

$$C_D = C_{D_o} + C_{D_\alpha}(\alpha) + C_{D_{\alpha^2}}(\alpha^2) + C_{D_{\delta_E}}(\delta_E) \tag{11}$$

$$C_m = C_{m_o} + C_{m_\alpha}(\alpha) + C_{m_{\delta_E}}(\delta_E) + \frac{\bar{c}}{2V} C_{m_q}(q) + \frac{\bar{c}}{2V} C_{m_{\dot{\alpha}}}(\dot{\alpha}) \tag{12}$$

The aerodynamic data used in this study represents a B727-type aircraft in the landing or takeoff configuration with the flaps deflected 30° and the landing gear extended. This data is given in Appendix A.

The unsteady terms for q and $\dot{\alpha}$ have been included because the aerodynamic forces on the aircraft take some finite amount of time to adjust to the changing wind conditions and aircraft configurations which occur when an aircraft encounters a thunderstorm wind field. The effect of these terms on aircraft dynamics is discussed in Etkin [10].

2.3 Pilot/Control System Models

The logic for three different control system models has been developed for simplified and meaningful simulation of controlled aircraft flight. The three control systems model the behavior of a typical pilot and two different autopilots. All three systems utilize throttle command rate to control thrust and thrust rate. The elevators of the B727 are used as control surfaces for pitch, vertical velocity, and flight path angle control. All three models use fixed gains for thrust rate and elevator angle adjustments during flight in varying winds. These gains can be adjusted for simulation of pilots of varying skill or autopilot control. Engine spool-up lag time due to turbomachinery lag and pilot thrust command delay have been included in the control system since instantaneous thrust command by the pilot does not provide instantaneous desired thrust. The pilot initiates a throttle rate command to control thrust and thrust rate. Because of the turbomachinery and pilot response lags, a predictive control scheme has been included. The purpose of this scheme is to provide some degree of lead since even the most responsive pilot must provide some lead in his throttle command because of turbomachinery lag. The turbomachinery lag time for an engine to reach full thrust from normal approach rpm can be as small as 2 sec and as high as 6 sec from idle rpm [11]. No characteristic lag

time was applied to elevator angle control since elevator response times are usually very small.

The B727 has three engines which deliver a total maximum thrust of 187,000 N (42,000 lbs) at takeoff at sea level and a minimum of 13,350 N (3,000 lbs) at forward idle. The maximum rate of thrust increase or decrease is on the order of 36,000 N/s (8,000 lbs/s) [12]. The thrust time constant (t_c) which describes the nonlinear time for thrust to advance from low power to full power at full setting could be as small as 2 sec [11].

The thrust control lag has been modeled assuming that the difference between the change of thrust and change of throttle setting can be expressed as a decaying exponential of the form

$$dF = \left\{1 - \exp\left[-\left(\frac{t - \tau}{t_c}\right)\right]\right\} d\Delta F \tag{13}$$

At time $t = \tau$, before the throttle is moved, the change in thrust is zero. At the time when the throttle is moved, a thrust change command ($d\Delta F$) is produced. At time $t = \tau + t_c$, dF produced by the throttle movement input is $(1 - 1/e)$ of the desired $d\Delta F$. At $t = \tau + 2t_c$, the change of thrust dF is $(1 - 1/e^2)$ of the desired $d\Delta F$ and exponentially approaches dF as $t \to \infty$.

The equation for thrust from $\tau = 0$ to $\tau = t$ allowing for continuous throttle movements included between $\tau = 0$ and $\tau = t$ is given by

$$F = F_o + \int_o^t \left\{1 - \exp\left[-\left(\frac{t - \tau}{t_c}\right)\right]\right\} \frac{d\Delta F}{d\tau} \, d\tau \tag{14}$$

where $d\Delta F/d\tau$ is the rate of change of throttle setting.

A more convenient form for Equation 14 than the integral form is a differential equation. Therefore, differentiating Equation 14 with respect to τ yields the following expression for $\dot{F}$ (rate change of thrust)

$$\dot{F} = \frac{1}{t_c} \int_o^t \exp\left\{-\left(\frac{t - \tau}{t_c}\right)\right\} \frac{d\Delta F}{d\tau} \, d\tau \tag{15}$$

so that

$$F + t_c\dot{F} = F_o + \int_o^t \frac{d\Delta F}{d\tau}\, d\tau \tag{16}$$

Differentiating Equation 16 further yields

$$\dot{F} + t_c\ddot{F} = \frac{d\Delta F}{d\tau}(t) \tag{17}$$

which can be written

$$\ddot{F} = \frac{\frac{d\Delta F}{d\tau}(t) - \dot{F}}{t_c} \tag{18}$$

where $\frac{d\Delta F}{d\tau}(t)$ is the rate change of throttle setting resulting from throttle movement by the pilot.

Three different control system models were investigated to simulate pilot or autopilot control. The first control system, model I, uses throttle setting control to initiate thrust rate control for controlling changes in aircraft ground speed. Elevator control is applied to correct for changes in vertical velocity and pitch angle. The control equation for thrust rate is given by

$$u = u_N + \frac{\partial u}{\partial \dot{x}}\left[(\dot{x} + t_c\ddot{x}) - \dot{x}_N\right] \tag{19}$$

where $u = \frac{d\Delta F}{d\tau}(t)$ is the rate of change of throttle setting commanded by the pilot's change in throttle position. In Equation 19, u_N corresponds to the trim throttle position change command which is always equal to zero at trim. The partial derivative, $\partial u/\partial \dot{x}$, is a fixed gain for pilot throttle rate command (by throttle position change) for changes in predicted aircraft ground speed $(\dot{x} + t_c\ddot{x})$ from the trim condition ground speed $\dot{x}_N$. The utilization of predicted ground speed enables the pilot or autopilot to compensate for the turbomachinery delay and for pilot/autopilot response lag. In this case, t_c = 5.0 sec (a relatively slow turbomachinery/pilot response lag time constant). The $\partial u/\partial \dot{x}$ gain used in this control system logic was set at -1,000 (N/s)/(m/s) which commands a $(\mp)$1,000 N/s thrust rate by throttle position movement for a 1 m/s

increase (decrease) in ground speed. It should be noted that u = 0 when the throttle is at idle or full-forward settings.

The control equation for elevator setting is given by

$$\delta_E = \delta_{E_N} + \frac{\partial \delta_E}{\partial \dot{z}} (\dot{z} - \dot{z}_N) + \frac{\partial \delta_E}{\partial \theta} (\theta - \theta_N) \tag{20}$$

where δ_E is the desired elevator setting and δ_{E_N} is the trim elevator setting. The fixed gains $\partial \delta_E / \partial \dot{z}$ and $\partial \delta_E / \partial \theta$ correspond to elevator angle commands due to changes in vertical velocity and pitch angle from the trim values, respectively. The $\partial \delta_E / \partial \dot{z}$ gain used in this control system model was set at 0.01 rad/(m/s) corresponding to an elevator angle command to pitch nose up (nose down) with 0.01 rad of elevator angle with 1 m/s increase (decrease) in sink rate. The $\partial \delta_E / \partial \theta$ gain used in this control system model was set at 0.1 rad/rad corresponding to an elevator angle command to pitch nose up (nose down) with 0.1 rad of elevator angle with 1 rad of nose pitch down (nose pitch up). It should be noted that the pilot/autopilot response characteristics can be altered or "fine-tuned" by changing the magnitudes of t_c or any of the three gains. Setting the three gains to zero corresponds to a fixed control mode of operation.

The second control system, model II, uses throttle setting control to initiate thrust rate control for controlling changes in the aircraft airspeed. Elevator control is applied to correct for changes in flight path angle and pitch angle. The control equation for thrust rate is given by

$$u = u_N + \frac{\partial u}{\partial V} [(V + t_c \dot{V}) - V_N] \tag{21}$$

where $u = \frac{d\Delta F}{\partial \tau}(t)$ is the rate change of throttle setting commanded by the pilot by change in throttle position, and $u_N = 0$ as noted previously in Equation 19. The partial derivative, $\partial u / \partial V$, is a fixed gain for pilot throttle rate command (by throttle position change) for changes in predicted aircraft airspeed $(V + t_c \dot{V})$ from the trim condition airspeed V_N. The $\partial u / \partial V$ gain used in this control system logic was set at -2,000 (N/s)/(m/s) which commands a $_{(\mp)}$2,000 N/s thrust rate by throttle

position movement for a 1 m/s increase (decrease) in airspeed and t_c = 2.0 sec.

The control equation for elevator setting is given by

$$\delta_E = \delta_{E_N} + \frac{\partial \delta_E}{\partial \dot{z}} (\dot{z} - \dot{z}_D) + \frac{\partial \delta_E}{\partial \theta} (\theta - \theta_N) \tag{22}$$

where δ_E, δ_{E_N}, $\partial \delta_E / \partial \dot{z}$, $\partial \delta_E / \partial \theta$ are defined as previously in Equation 20. Flight path angle is maintained by vertical velocity control through elevator angle control. To maintain a desired flight path angle of approximately 3 degrees, the pilot must attain a desired vertical velocity $\dot{z}_D$ equal to:

$$z_D = -\dot{x}(0.052) \tag{23}$$

where $\dot{x}$ is the instantaneous aircraft ground speed and 0.052 is approximately tan (3°). The gains $\partial \delta_E / \partial \dot{z}$ and $\partial \delta_E / \partial \theta$ were set to 0.01 rad/(m/s) and 0.1 rad/rad, respectively. This system works well when the aircraft is held relatively close to the glide slope beam and the flight path angles are kept within reasonable limits. However, when the aircraft deviates a large distance above or below the glide slope for a relatively long time period, the logic of tracking a 3° glide slope beam is insufficient for landing at the touchdown point.

The third control system, model III, controls airspeed by throttle rate application, with touchdown point and pitch attitude controlled by elevator angle control. The control equation for the thrust rate is given by Equation 21 of the previously mentioned airspeed control system. A turbomachinery/pilot response lag time constant t_c was set at 3 seconds and the thrust rate gain $\partial u / \partial V$ was set at -1,000 (N/s)/(m/s). The control equation for elevator angle control is the same as that in the previous control system given by Equation 22. However, in this case, z_D, the desired vertical velocity is determined by the aircraft's position above or below the glide slope. If the aircraft is above the glide slope, z_D is determined by the flight path angle needed to land at the horizontal touchdown point x_L. This relationship is given by:

$$z_D = -\dot{x}\left(\frac{z}{x_L - x}\right) \tag{24}$$

where $\dot{x}$ is the aircraft ground speed and z and x are aircraft vertical position and horizontal position, respectively. If the aircraft falls below the glide slope, the control system schedules a 1° ascent flight path angle to reintercept the glide slope, rather than fly a shallow flight path angle to touchdown at x_L. The desired ascent rate for a 1° glide slope intercept is given by

$$z_D = \dot{x}(0.0174) \tag{25}$$

where $\dot{x}$ is aircraft ground speed and 0.0174 is approximately tan (1°). The elevator control gains $\partial\delta_E/\partial\dot{z}$ and $\partial\delta_E/\partial\theta$ were set at 0.015 (rad)/(m/s) and 0.1 rad/rad, respectively.

CHAPTER 3. FLIGHT PATH DETERIORATION PARAMETERS

In order to assess the potential severity of a longitudinal wind shear hazard existing along the flight path, some quantitative parameters are needed to describe the response of the aircraft/pilot system. These parameters are called the flight path deterioration parameters (FPDP) and they describe the aircraft trajectory by glide slope deviations and airspeed deviations from reference airspeed. The Doppler-measured longitudinal glide slope winds are fed into the microprocessor containing the aircraft trajectory program and a simulated trajectory is calculated. The FPDP would then be computed by the program to describe the aircraft's deviations from the glide slope and reference airspeed. These parameters would be displayed to the controller or pilot and a decision as to whether or not to attempt takeoff or landing along the glide slope monitored by the wind shear warning system could be made before the aircraft encounters the monitored area. Naturally, there exists a need to determine the safety limits of these parameters so that the pilot or controller can make a go/no-go decision based on the parameters displayed by the warning and detection system. It should be noted that the parameters used in this study are basically for analysis purposes--they may not be the most informative data that a pilot or controller can relate to a safe approach or takeoff. However, it is anticipated that the final parameters used in the actual system will be based on similar analytical parameters.

The proposed flight path deterioration parameters for flight path and airspeed deviation were devised using the following logic. Normalized altitude, HP/HG, was chosen as the flight path deviation parameter where HP is the height of the aircraft above the ground and HG is the height of the glide slope above the ground. This formulation was chosen over $\Delta H = HP - HG$ because it accounts for the fact that altitude deviations become more serious at lower altitudes than at higher altitudes.

The airspeed deviation parameter chosen was simply the deviation of airspeed from the reference value. However, in both flight path and airspeed parameters, the positive deviations are examined separately from the negative deviations to avoid the cancellation errors. Although an averaging technique is used, it is believed that this method provides more meaningful results than root mean square averaging.

In summary, the FPDP used in this analysis and illustrated in Figure 4 are:

1. Flight path deviation

a) $GS+ = \frac{1}{n} \sum_{i=1}^{n} \frac{HP_i}{HG_i}$

HP_i = height of aircraft above ground at point i

HG_i = height of glide slope above ground at point i

where HP_i/HG_i above or on glide slope ≥ 1.0

n = number of points aircraft is above glide slope

The points are taken at 1 sec intervals.

b) $GS- = \frac{1}{m} \sum_{i=1}^{m} \frac{HP_i}{HG_i}$

where HP_i/HG_i below glide slope < 1.0

m = number of points aircraft is below glide slope.

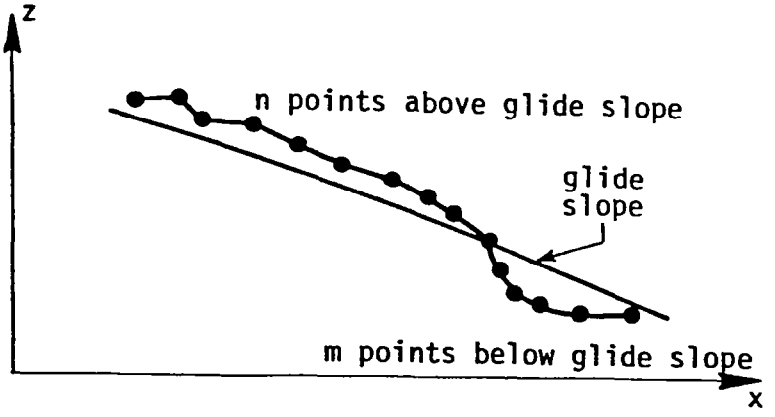

Figure 4 Concept of flight path deterioration parameters (FPDP).

2. Airspeed deviation

a) $V+ = \frac{1}{j} \sum_{i=1}^{j} (V_i - V_{ref})$

V_i = aircraft airspeed at point i

V_{ref} = reference airspeed

where $(V_i - V_{ref}) \geq 0$

j = number of points aircraft airspeed (V_i) is above V_{ref}

b) $V- = \frac{1}{k} \sum_{i=1}^{k} (V_i - V_{ref})$

where $(V_i - V_{ref}) < 0$

k = number of points aircraft airspeed (V_i) is below V_{ref}.

A detailed example illustrating the calculation of the FPDP is given in Appendix B.

CHAPTER 4. RESULTS OF COMPUTER AND SIMULATOR STUDIES

4.1 Description of Test Plan

In an effort to determine if the aircraft trajectory model simulates a real aircraft/pilot system, the results of the trajectory program were compared with a series of runs that were carried out in the B727 simulator at the NASA Ames Research Center (NASA Ames). The simulated aircraft was flown through three different wave-form wind models characteristic of a thunderstorm downburst cell environment (Figure 5). The simulator runs were designed to test aircraft/pilot response to longitudinal and vertical wind waves of varying amplitudes and frequencies. The test plan appears in Table 1 and a summary of the computer and simulator results that will be discussed below is included in Tables 2 and 3, respectively.

4.2 Illustration of Aircraft Sensitivity to Longitudinal Wind Shears at Various Frequencies

Before discussion of the results of the aforementioned computer and simulation tests, it is desirable to examine the response of the fixed-control aircraft (no pilot input) to winds described as longitudinal sine waves of constant amplitude but different frequencies using the aircraft trajectory program as developed in this study. This will serve to illustrate the hypotheses of McCarthy, Blick, and Bensch [3], and Frost and Crosby [4] stating that fixed-control aircraft are most sensitive to longitudinal wind shears occurring at approximately the aircraft's phugoid frequency. The following tests were made using the aircraft trajectory model with an airplane characteristic of a B727. The aircraft was trimmed (flaps 30°) for flight along a 2.9° flight path with an approach airspeed of 75.1 m/s and an angle of attack of 4.7°. In all cases the wave is encountered at $x = 0.0$ m. Figure 6a shows the trajectory of an aircraft characteristic of a B727 encountering a 5.15 m/s (10 kt) full head wind to tail wind sine wave at the phugoid frequency

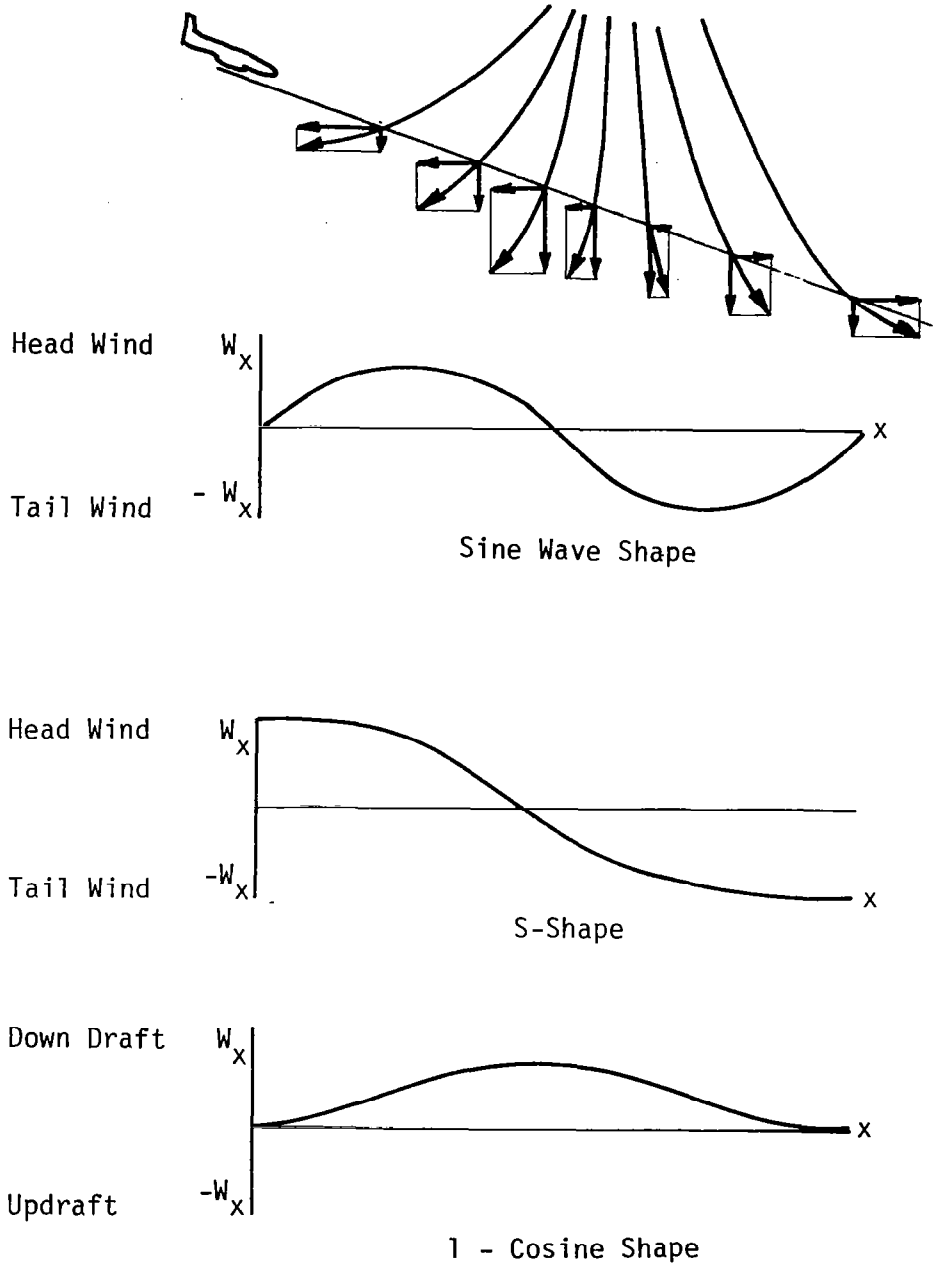

Figure 5 Wind models used to simulate a thunderstorm downburst cell.

TABLE 1 Test Plan for Simulator and Computer Runs.

	Amplitude	Frequency
Aircraft trimmed for: 3.0° glide slope 70.0 m/s airspeed 63,958 kg (140,000 lbs) gear down, flaps 30°		
S-shape head wind to tail wind shear wave	5.15 m/s (10 kts)	ω_{ph} (≈38 sec)
	10.30 m/s (20 kts)	ω_{ph} (≈38 sec)
	15.45 m/s (30 kts)	ω_{ph} (≈38 sec)
	15.45 m/s	$2\omega_{ph}$ (≈19 sec)
	15.45 m/s	$1/2\ \omega_{ph}$ (≈76 sec)
Full sine wave head wind to tail wind shear	5.15 m/s	ω_{ph}
	10.30 m/s	ω_{ph}
	15.45 m/s	ω_{ph}
	20.60 m/s	ω_{ph}
	20.60 m/s	$2\ \omega_{ph}$
	20.60 m/s	$1/2\ \omega_{ph}$
1 - cosine down draft	5.15 m/s (17 ft/s)	ω_{ph}
	10.30 m/s (34 ft/s)	ω_{ph}
	15.45 m/s (51 ft/s)	ω_{ph}
	15.45 m/s (51 ft/s)	$2\ \omega_{ph}$
	15.45 m/s (51 ft/s)	$1/2\ \omega_{ph}$
Combinations:		
S-shape, 0-5.15 m/s tail wind shear at ω_{ph} 1 - cosine, 5.15 m/s (17 ft/s) downburst at ω_{ph}		
S-shape, 0-10.3 m/s tail wind shear at ω_{ph} 1 - cosine, 10.3 m/s (34 ft/s) downburst at ω_{ph}		
S-shape, 0-20.6 m/s tail wind shear at ω_{ph} 1 - cosine, 20.6 m/s (68 ft/s) downburst at ω_{ph}		
S-shape, 0-20.6 m/s tail wind shear at $2\ \omega_{ph}$ 1 - cosine, 20.6 m/s (68 ft/s) downburst at $2\ \omega_{ph}$		

TABLE 2 Flight Trajectory Computer Run Summary.

Figure	Control System	Wave Shape	Direction	Amplitude (m/s)	Frequency (ω_{ph})	V_{air} (m/s) (min,max)	α (Deg) (min,max)	V+ (m/s)	V- (m/s)	GS+	GS-	F/F_{max}* (min,max)
6a	Fixed	Sine	Longitudinal	5.15	1.0	65, 88	3.7, 6.1	5.02	-5.93	1.32	0.56	0.35, 0.35
6b	Fixed	Sine	Longitudinal	5.15	2.0	67, 80	4.2, 5.9	2.78	-3.68	1.11	0.76	0.35, 0.35
6c	Fixed	Sine	Longitudinal	5.15	0.5	71, 79	4.4, 5.2	1.92	-2.37	2.48	0.13	0.35, 0.35
7a	Pilot	Sine	Longitudinal	5.15	1.0	73, 79	3.8, 5.4	1.54	-1.52	1.05	0.84	0.21, 0.47
7b	Pilot	Sine	Longitudinal	5.15	2.0	70, 79	3.8, 5.9	0.97	-1.24	1.02	0.97	0.30, 0.41
7c	Pilot	Sine	Longitudinal	5.15	0.5	71, 78	3.8, 5.8	2.40	-2.56	1.30	1.00	0.16, 0.51
8a	Pilot	Sine	Longitudinal	5.15	1.0	63.7, 81.2	3.4, 8.5	4.01	-3.57	1.09	0.78	I, 0.83
8b	Pilot	Sine	Longitudinal	10.30	1.0	59.8, 89.6	1.8, 10.0	7.09	-4.78	1.26	0.83	I, 1.0
8c	Pilot	Sine	Longitudinal	15.45	1.0	56.9, 93.8	1.1, 11.4	8.99	-6.09	1.40	0.79	I, 1.0
10a	Pilot	Sine	Longitudinal	20.60	1.0	54.4, 97.0	0.6, 12.6	10.80	-7.10	1.50	0.73	I, 1.0
10b	Pilot	Sine	Longitudinal	20.60	2.0	45.4, 88.7	0.1, Stall	9.00	-7.40	1.07	0.69	I, 1.0
10c	Pilot	Sine	Longitudinal	20.60	0.5	63.0, 84.0	2.9, 8.7	4.97	-3.71	1.77	0.94	I, 0.95
12a	Pilot	1-Cosine	Downburst	5.15	1.0	67.0, 74.0	5.0, 7.4	1.97	-1.63	1.0	0.81	0.11, 0.66
12b	Pilot	1-Cosine	Downburst	10.30	1.0	69.3, 78.7	3.8, 8.0	4.05	-2.77	1.0	0.79	I, 1.0
12c	Pilot	1-Cosine	Downburst	15.45	1.0	63.0, 80.1	3.4, 8.7	5.28	-3.66	1.0	0.60	I, 1.0
14b	Pilot	1-Cosine	Downburst	15.45	2.0	60.5, 81.8	3.0, 10.3	5.24	-3.89	1.0	0.75	I, 1.0
14c	Pilot	1-Cosine	Downburst	15.45	0.5	66.6, 70.1	6.2, 7.3	0.67	-1.89	1.0	0.69	0.33, 1.0
16a	Pilot	S-Shape	Longitudinal	5.15	1.0	68.3, 72.1	5.6, 6.9	1.13	-0.91	1.07	0.98	0.20, 0.53
16b	Pilot	S-Shape	Longitudinal	10.30	1.0	66.3, 74.4	5.0, 7.6	2.21	-1.84	1.10	0.95	0.73, 1.0
16c	Pilot	S-Shape	Longitudinal	15.45	1.0	65.3, 76.4	4.4, 8.0	3.36	-2.15	1.24	0.95	I, 0.87
18b	Pilot	S-Shape	Longitudinal	15.45	2.0	62.1, 81.8	3.1, 9.0	5.63	-3.79	1.12	0.83	I, 1.0
18c	Pilot	S-Shape	Longitudinal	15.45	0.5	69.2, 71.4	5.8, 6.5	0.85	-0.31	1.60	0.98	0.27, 0.55
21	Pilot	1-Cosine	Downburst	5.15	1.0							
		S-Shape	Longitudinal	5.15	1.0	66.2, 75.4	4.6, 7.6	2.53	-1.93	1.01	0.84	I, 0.75
22a	Pilot	1-Cosine	Downburst	10.30	1.0							
		S-Shape	Longitudinal	10.30	1.0	64.5, 80.5	3.5, 8.2	5.28	-3.04	1.00	0.80	I, 1.0
22b	Pilot	1-Cosine	Downburst	20.60	1.0							
		S-Shape	Longitudinal	20.60	1.0	54.3, 70.1	6.0, 13.3	0.76	-9.00	1.00	0.67	0.35, 1.0
22c	Pilot	1-Cosine	Downburst	20.60	2.0							
		S-Shape	Longitudinal	20.60	2.0	49.8, 75.9	6.3, 16.0	2.89	-10.39	1.00	0.62	0.35, 1.0
24	Auto-Pilot III	Sine	Longitudinal	15.45	1.0	56.9, 88.5	-0.3, 12.7	7.40	-5.52	1.44	0.86	I, 1.0

*I = idle thrust.

TABLE 3 Flight Trajectory Simulator Run Summary.

Figure	Control System	Wave Shape	Direction	Amplitude (m/s)	Frequency (ω_{ph})	V_{air} (m/s) (min,max)	α (Deg) (min,max)	V+ (m/s)	V- (m/s)	GS+	GS-	Throttle, Throttle Position, Position$_{max}$ (min,max)
9a	Pilot	Sine	Longitudinal	5.15	1.0	67.0,74.2	3.2,6.0	1.75	-0.70	1.00	0.98	0.08,0.88
9b	"	"	"	10.30	1.0	58.8,77.3	2.5,10.5	3.19	-4.30	1.00	0.99	0.02,1.0
9c	"	"	"	15.45	1.0	61.3,85.0	-0.3,8.7	6.85	-5.30	1.00	0.95	0.12,1.0
11a	"	"	"	20.60	1.0	61.9,89.6	-0.9,8.2	9.69	-4.20	1.01	0.94	0.06,1.0
11b	"	"	"	20.60	2.0	50.0,86.6	-1.0,18.5	6.55	-4.47	1.01	0.94	0.17,0.88
11c	"	"	"	20.60	0.5	64.9,85.6	0.2,6.6	7.06	-1.84	1.02	0.87	0.25,1.0
13a	Pilot	1-Cosine	Downburst	5.15	1.0	67.0,71.1	4.2,6.4	1.10	-0.52	1.00	0.99	0.25,0.65
13b	"	"	"	10.30	1.0	66.5,70.6	4.2,6.3	0.66	-0.79	1.00	0.99	0.25,1.0
13c	"	"	"	15.45	1.0	66.5,70.6	2.9,7.4	0.85	-1.02	1.00	0.97	0.29,1.0
15b	"	"	"	15.45	2.0	64.4,74.7	1.0,9.3	2.27	-2.05	1.00	0.97	0.22,1.0
15c	"	"	"	15.45	0.5	67.5,70.1	3.7,6.0	0.57	-0.71	1.00	0.94	0.25,1.0
17a	Pilot	S-Shape	Longitudinal	5.15	1.0	67.0,70.1	4.6,6.1	0.45	-0.58	1.01	0.94	0.25,0.75
17b	"	"	"	10.30	1.0	67.0,70.6	4.4,5.8	0.62	-0.88	1.03	0.99	0.26,0.61
17c	"	"	"	15.45	1.0	66.5,70.6	4.2,6.1	0.66	-0.96	1.04	0.95	0.23,0.83
19b	"	"	"	15.45	2.0	62.4,72.0	3.5,8.2	0.88	-2.00	1.03	0.91	0.0,1.0
19c	"	"	"	15.45	0.5	67.5,70.4	4.3,5.9	0.58	-0.80	1.07	0.93	0.28,0.52
-- *	Pilot	1-Cosine	Downburst	5.15	1.0							
		S-Shape	Longitudinal	5.15	1.0	67.8,69.7	4.7,5.6	-	-	-	-	0.28,0.66
23a	Pilot	1-Cosine	Downburst	10.30	1.0							
		S-Shape	Longitudinal	10.30	1.0	64.3,69.9	4.4,7.4	0.63	-2.18	1.00	0.98	0.30,1.0
23b	Pilot	1-Cosine	Downburst	20.60	1.0							
		S-Shape	Longitudinal	20.60	1.0	57.4,88.0	2.3,13.2	6.39	-4.12	1.00	0.78	0.30,1.0
23c	Pilot	1-Cosine	Downburst	20.60	2.0							
		S-Shape	Longitudinal	20.60	2.0	50.8 77.5	1.4,19.1	3.48	-5.09	1.00	0.81	0.28,1.0

*Case missing.

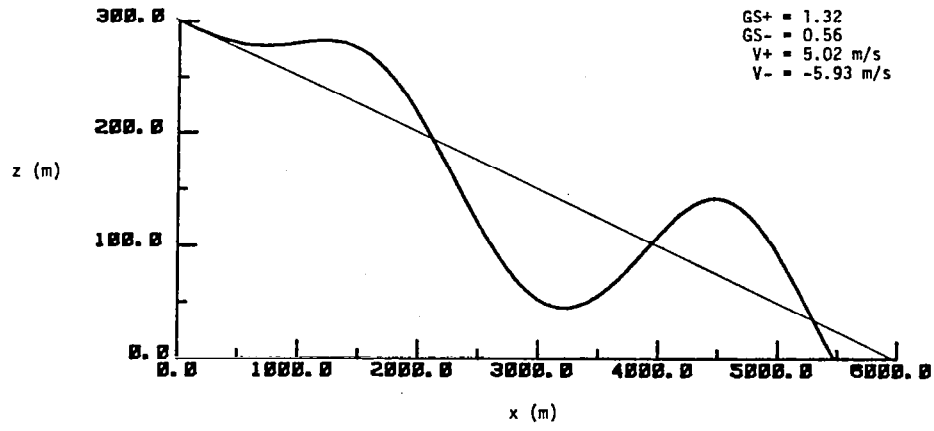

a) Simulated trajectory through a longitudinal sine wave of 5.15 m/s amplitude and ω_{ph} frequency.

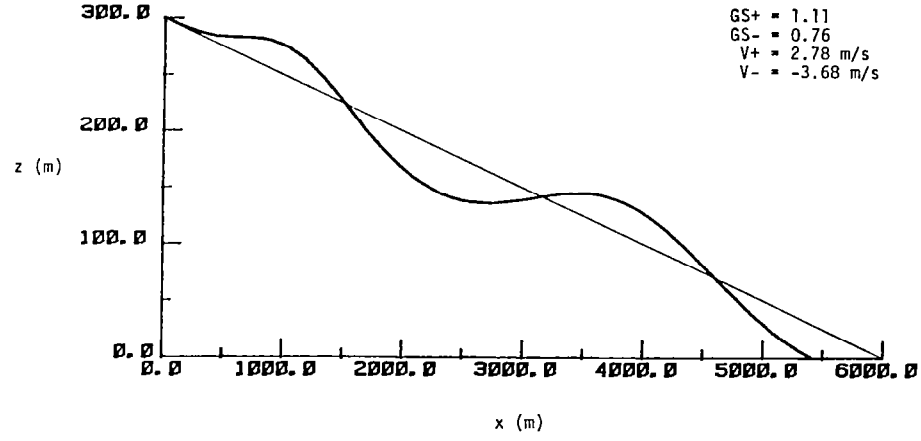

b) Simulated trajectory through a longitudinal sine wave of 5.15 m/s amplitude and 2 ω_{ph} frequency.

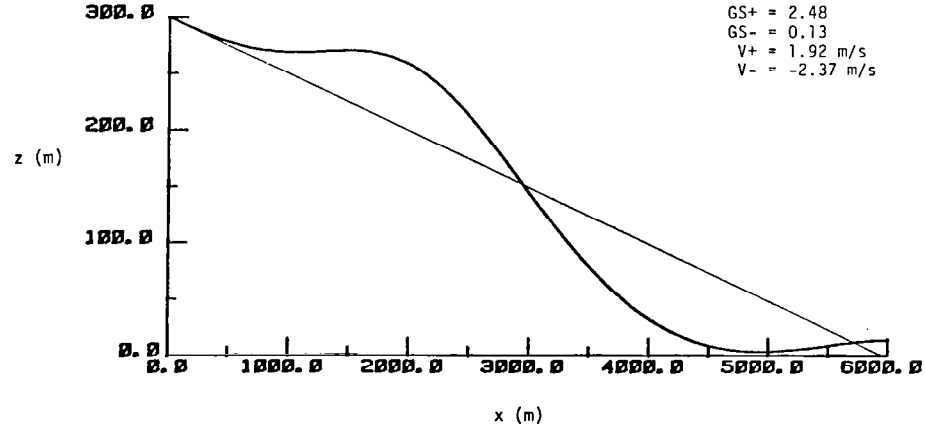

c) Simulated trajectory through a longitudinal sine wave of 5.15 m/s amplitude and 1/2 ω_{ph} frequency.

Figure 6 Computer-simulated approach trajectory of a B727 with fixed controls through a longitudinal sine wave wind.

(≈38 sec) [3]. The encounter with the increasing head wind caused the aircraft to initially float above the glide slope. The encounter with the decreasing head wind to increasing tail wind portion of the wave caused a drastic decrease in airspeed of approximately 11 m/s (21.4 kts) causing the aircraft to drop below the glide slope. The aircraft then picked up airspeed during its descent below the glide slope and subsequently ascended above the glide slope. Thus, the encounter with the longitudinal shear wave excited an airspeed oscillation thereby causing flight path deviation. In this case, the airspeed ranged between 65 m/s and 88 m/s and angle of attack ranged between 3.7° and 6.1°. The airspeed deterioration parameters for this case were V+ = 5.02 m/s and V- = -5.93 m/s. Figure 6b shows the trajectory of the fixed-control B727 encountering a 5.15 m/s (10 kt) head wind to tail wind sine wave at 2 ω_{ph} (≈19 sec). The aircraft remains in the wave for a shorter period of time than in the aforementioned case so that aircraft inertia is able to overcome some of the effect of the wave on airspeed. In this case, airspeed ranged between 67 m/s and 80 m/s and angle of attack ranged between 4.2° and 5.9°. The airspeed deterioration parameters were V+ = 2.78 m/s and V- = -3.68 m/s, which are of lower magnitude than for the phugoid period case. These parameters indicate lower airspeed variation for the 2 ω_{ph} wave than for the ω_{ph} wave, and therefore less flight path deviation. Figure 6c shows the trajectory of a B727 encountering a 5.15 m/s (10 kt) head wind to tail wind sine wave at 1/2 ω_{ph}. The deviations from the glide slope are misleadingly large for this case because the aircraft remains out of trim for a longer period than for the two previous runs. However, the airspeed ranged between 71 m/s and 79 m/s and angle of attack varied from 4.4° to 5.2°. The airspeed deterioration parameters for this case were V+ = 1.9 m/s and V- = -2.37 m/s. Thus, the airspeed deterioration parameters were largest for the ω_{ph} wave, indicating that the airspeed oscillations excited by the longitudinal shear wave will be largest for waves at the phugoid frequency.

Figure 7 shows the computed trajectories with simulated pilot control through ω_{ph}, 2 ω_{ph}, and 1/2 ω_{ph} sine waves, respectively. The ground speed/vertical velocity control system I described in Section 2.3 was used in these cases. It can be seen that the excessive flight path

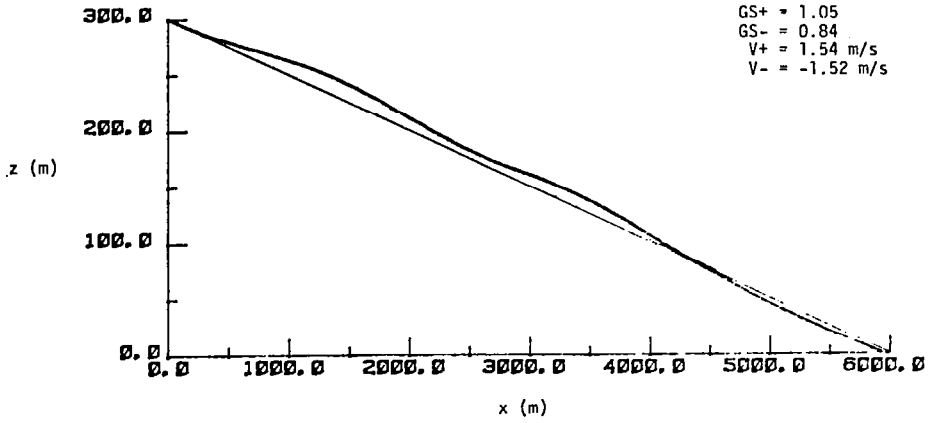

a) Simulated trajectory through a longitudinal sine wave of 5.15 m/s amplitude and ω_{ph} frequency.

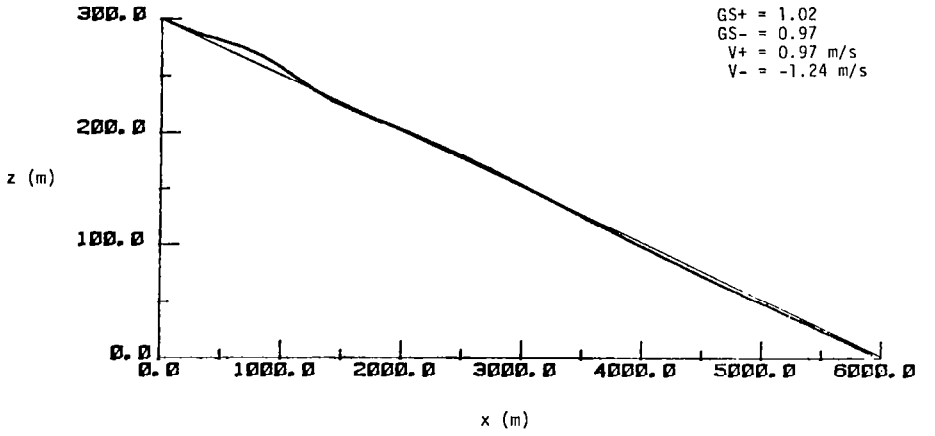

b) Simulated trajectory through a longitudinal sine wave of 5.15 m/s amplitude and 2 ω_{ph} frequency.

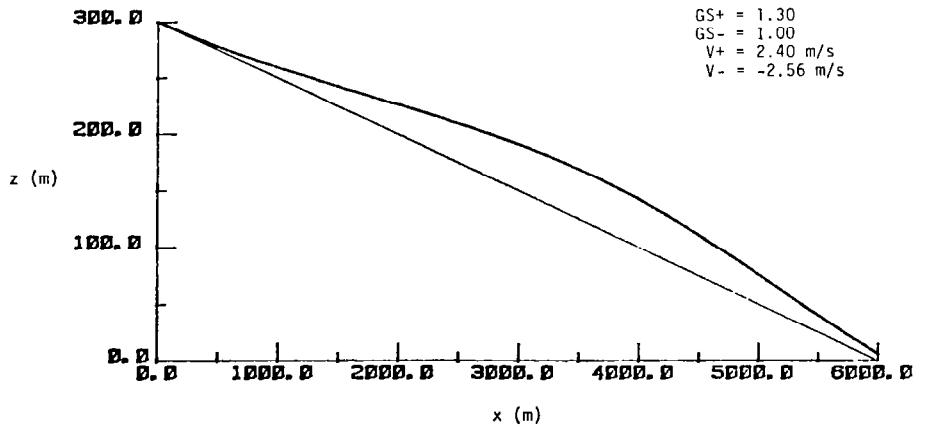

c) Simulated trajectory through a longitudinal sine wave of 5.15 m/s amplitude and 1/2 ω_{ph} frequency.

Figure 7 Computer-simulated approach trajectory of a B727 using control system I through a longitudinal sine wave wind.

deviations of the preceding fixed-control runs have been dramatically lessened. In all cases, the aircraft remained on or above the glide slope for most of the run. A comparison between the ω_{ph} and 2 ω_{ph} cases shows less flight path and airspeed deviation for the 2 ω_{ph} case than for the ω_{ph} case, which is to be expected following the results of the fixed-control trajectories. However, for the 1/2 ω_{ph} case, the aircraft ballooned above the glide slope and began to recover towards the end of the run. The ballooning and greater spread of airspeed deviation is due to the aircraft being in the wind for a longer duration, whereas the ω_{ph} and 2 ω_{ph} winds are relatively transient.

4.3 Computed Aircraft Trajectory Results

The following cases were run using the test plan described in Section 4.1. In all cases the B727 aircraft was trimmed (flaps 30°) for a 3.0° glide path angle with an approach airspeed of 70 m/s and an angle of attack of 6.2°. All wind profiles are encountered at x = 0.0 m. The flight profiles of the test pilot simulator runs have also been included in this section for comparison purposes. They are described in detail in Chapter 5. The four flight path deterioration parameters pertaining to each case are given on each trajectory plot.

The airspeed/flight path angle control system II described in Section 2.3 was used in these cases. It should be noted that the fixed gains used in the formulation of this model represent an initial effort to model pilot control response to wind shear profiles and to simulate engine response characteristics.

4.3.1 Sine Waves

1. 5.15 m/s at ω_{ph}. Figure 8a shows the simulated trajectory of a B727 through a 5.15 m/s head wind to tail wind sine wave at ω_{ph}. The aircraft balloons above the glide slope when encountering the increasing head wind portion of the wave. The pilot attempts to lower the thrust and pitch down to remain on the 3° glide slope. However, the aircraft next encounters the head wind to tail wind portion of the wave and is caught in a decreasing airspeed situation with low thrust and the nose pitched down. The pilot must then pitch the nose up and increase thrust

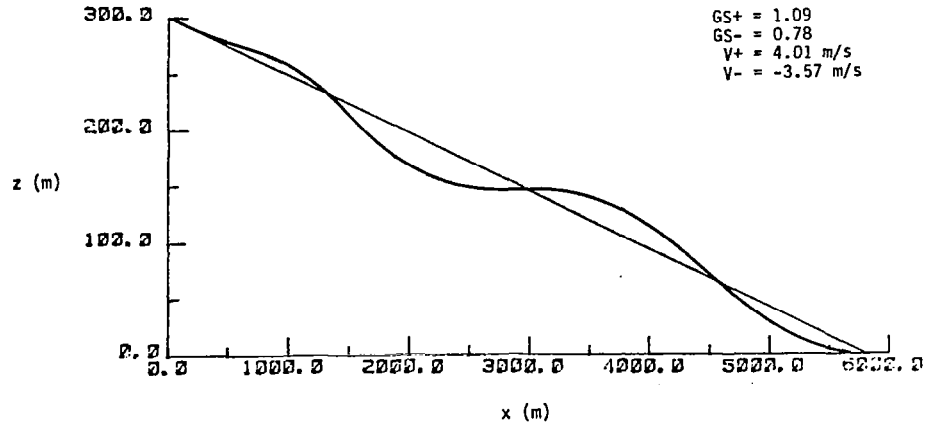

a) Simulated trajectory through a longitudinal sine wave of 5.15 m/s amplitude and ω_{ph} frequency.

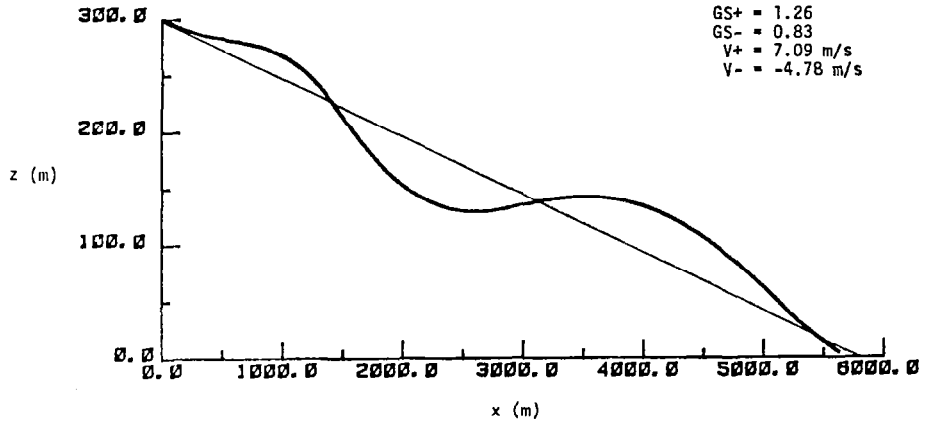

a) Computer-simulated trajectory using control system II.

b) Simulated trajectory through a longitudinal sine wave of 10.3 m/s amplitude and ω_{ph} frequency.

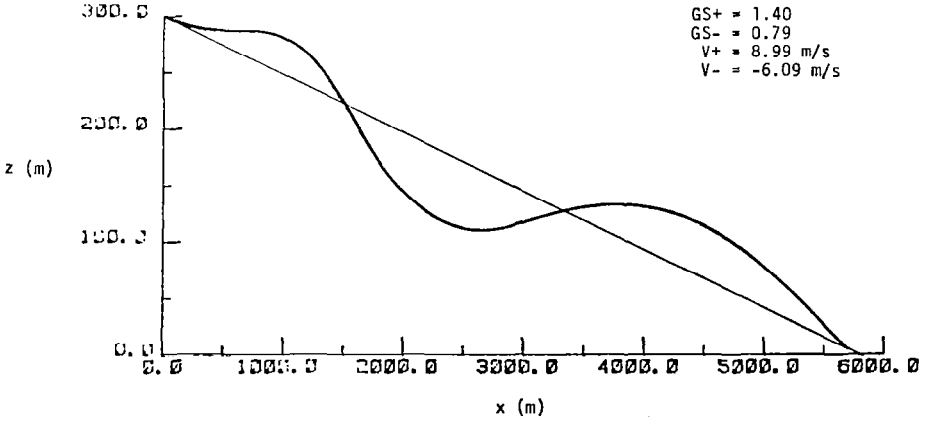

c) Simulated trajectory through a longitudinal sine wave of 15.45 m/s amplitude and ω_{ph} frequency.

Figure 8 Computer-simulated approach trajectory of a B727 using control system II through a longitudinal sine wave wind.

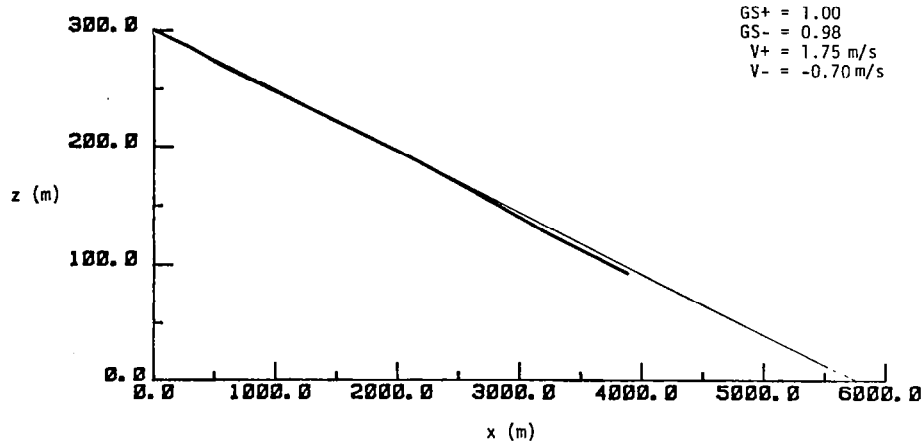

a) Simulated trajectory through a longitudinal sine wave of 5.15 m/s amplitude and ω_{ph} frequency.

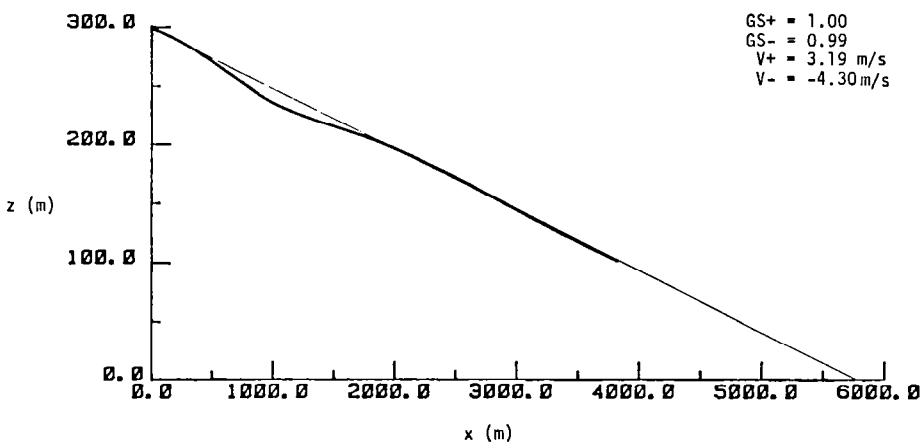

b) Simulated trajectory through a longitudinal sine wave of 10.3 m/s amplitude and ω_{ph} frequency.

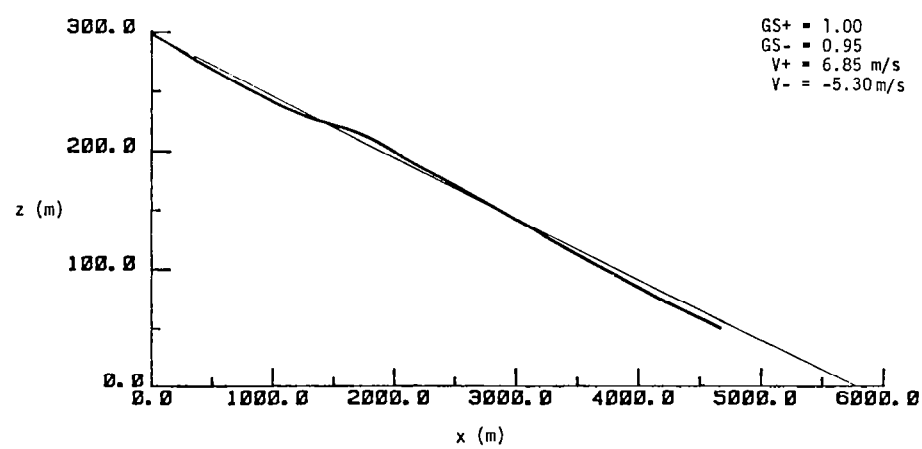

c) Simulated trajectory through a longitudinal sine wave of 15.45 m/s amplitude and ω_{ph} frequency.

Figure 9 Approach trajectory of a B727 aircraft performed by a test pilot in the NASA Ames simulator through a longitudinal sine wave wind.

to arrest the increased sink rate and to damp out the "roller coaster" effect of the longitudinal shear wave. The aircraft then reintercepts and drops below the glide slope at the termination of the run. However, it can be seen that the "roller coaster" effect is being damped out by pilot control. The amount of damping the pilot can apply is dependent upon the altitude at which the wave is encountered, which in this case is a relatively low 300 m. The airspeed varied from 63.7 m/s to 81.2 m/s, angle of attack varied from 3.4° to 8.5°, and thrust ranged from idle to approximately 83 percent full forward.

2. 10.3 m/s at ω_{ph}. Figure 8b shows the simulated trajectory of a B727 through a 10.3 m/s sine wave at ω_{ph}. A comparison of the airspeed deterioration parameters reveals that the airspeed deviations are greater for the 10.3 m/s wave amplitude than for the 5.15 m/s amplitude, which is to be expected. The flight path deviation parameter spread [(GS+) - (GS-)] is larger for the 10.3 m/s wave than for the 5.15 m/s wave which is also to be expected. For this run, the airspeed ranged between 59.8 m/s and 89.6 m/s and angle of attack varied between 1.8° and 10.0°. Thrust varied from idle to full forward.

3. 15.45 m/s at ω_{ph}. Figure 8c shows the flight path of a B727 flown through a 15.45 m/s sine wave at ω_{ph}. The flight path deviation spread has again increased and the airspeed deviation parameters have also increased. Airspeed ranged between 56.9 m/s and 93.8 m/s and angle of attack varied between 1.1° and 11.4°. Thrust ranged from idle to full forward.

4. 20.6 m/s at ω_{ph}. The flight path of a B727 flown through a 20.6 m/s longitudinal sine wave at ω_{ph} is given in Figure 10a. Again, the GS+/GS- spread has increased and the airspeed parameters have increased. The airspeed varied between 54.4 m/s and 97.0 m/s, angle of attack ranged between 0.6° and 12.6° and thrust varied from idle to full forward.

5. 20.6 m/s at 2 ω_{ph}. The trajectory of a B727 flown through a 20.6 m/s sine wave at 2 ω_{ph} is given in Figure 10b. The aircraft underwent large airspeed deviations within a short time span and attempts to control the airspeed resulted in the aircraft entering the stall regime. Therefore, the trajectory is probably invalid past x = 1,000.0 m where

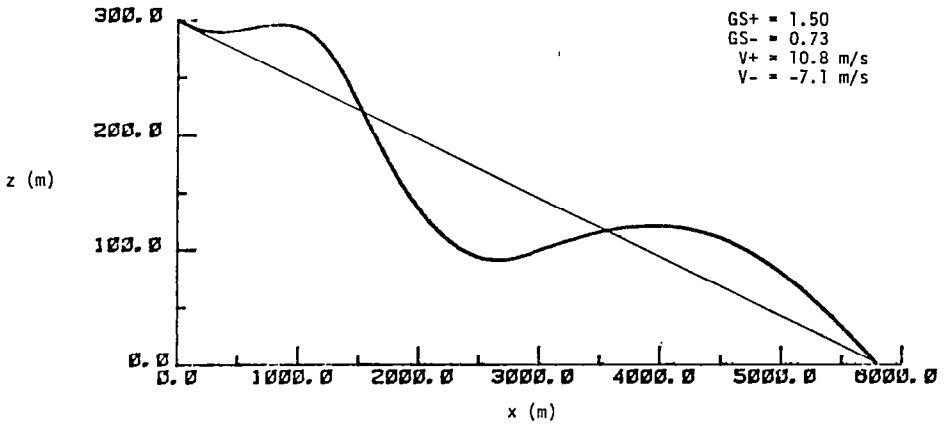

a) Simulated trajectory through a longitudinal sine wave of 20.6 m/s amplitude and ω_{ph} frequency.

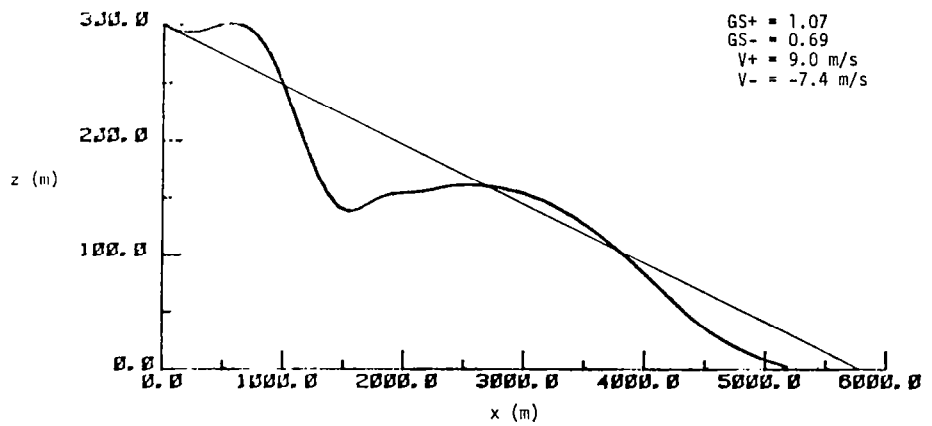

b) Simulated trajectory through a longitudinal sine wave of 20.6 m/s amplitude and 2 ω_{ph} frequency.

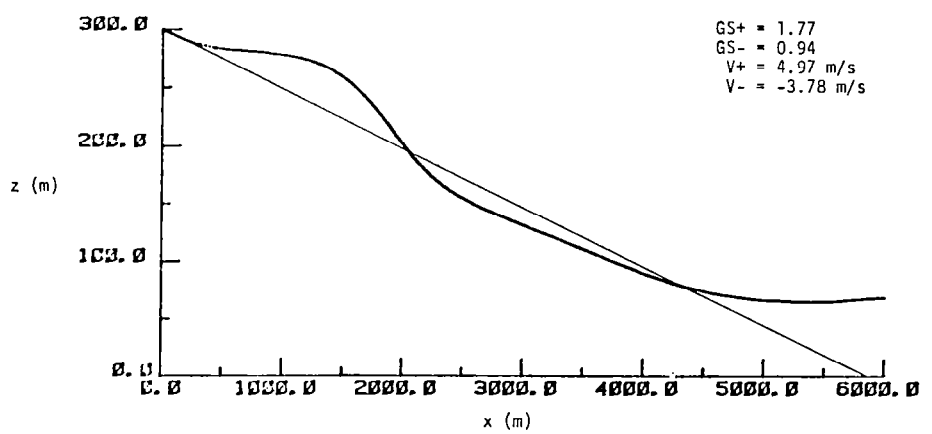

c) Simulated trajectory through a longitudinal sine wave of 20.6 m/s amplitude and 1/2 ω_{ph} frequency.

Figure 10 Computer-simulated approach trajectory of a B727 using control system II through a longitudinal sine wave wind.

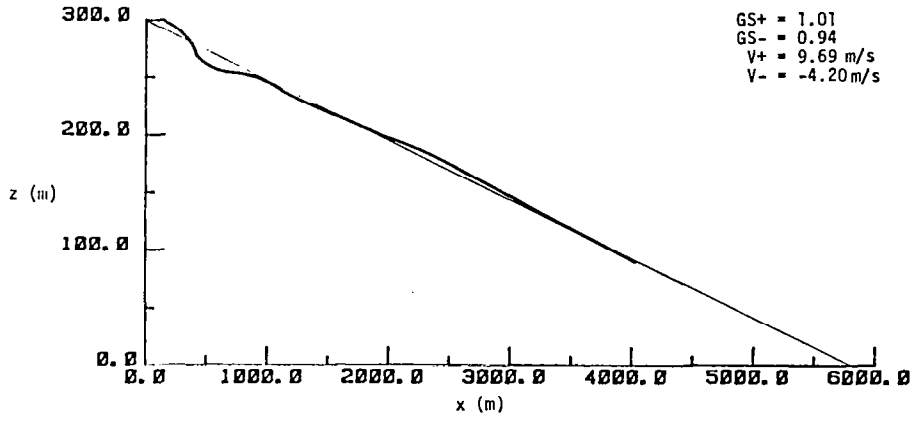

a) Simulated trajectory through a longitudinal sine wave of 20.6 m/s amplitude and ω_{ph} frequency.

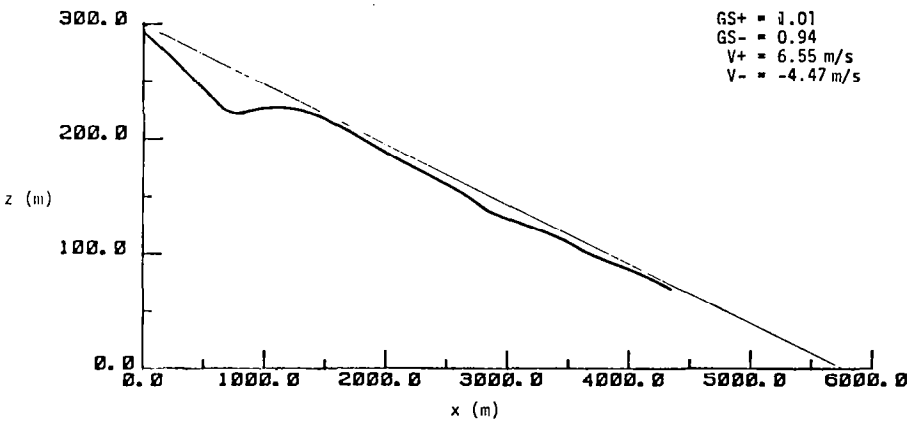

b) Simulated trajectory through a longitudinal sine wave of 20.6 m/s amplitude and 2 ω_{ph} frequency.

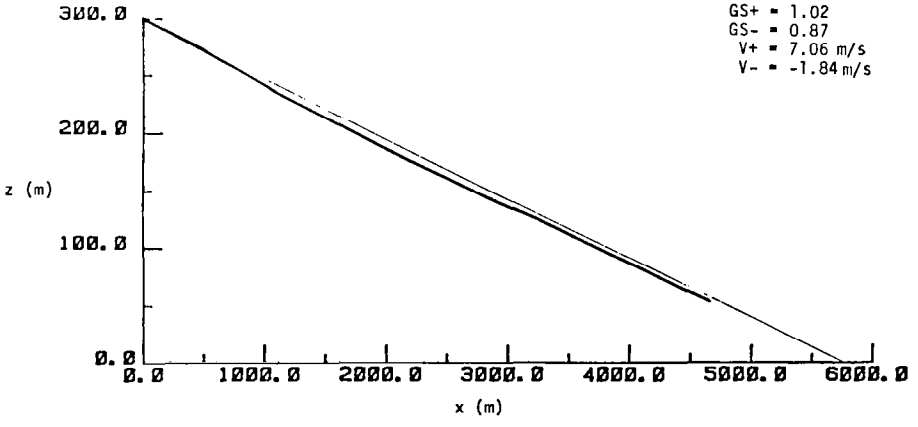

c) Simulated trajectory through a longitudinal sine wave of 20.6 m/s amplitude and 1/2 ω_{ph} frequency.

Figure 11 Approach trajectory of a B727 aircraft performed by a test pilot in the NASA Ames simulator through a longitudinal sine wave wind.

the thrust was decreased to idle to bleed off the airspeed increase and the head wind to tail wind shear reached a maximum. Airspeed reaches a minimum of 45.4 m/s. This resulted in a descent rate and stall condition which probably would have been beyond the pilot's recovery ability due to the low altitude. Although the results of this case are contradictory to the hypothesis that the phugoid frequency waves are more severe than waves of other frequencies, the authors believe that a large wind gradient due to large amplitude and short wave length may be detrimental to a safe approach. It appears that wave amplitude is an important factor in flight path deterioration within some frequency bandwidth bracketing the phugoid frequency. The extent of this bandwidth requires further investigation. In summary, the large wind gradient and the attempt to overcome it clearly put the aircraft in a dangerous flight regime.

6. 20.6 m/s at 1/2 ω_{ph}. Figure 10c shows the trajectory of a B727 flown through a 20.6 m/s sine wave at 1/2 ω_{ph}. The aircraft encounters the steadily increasing head wind and rises above the glide slope. The airspeed increase is soon arrested by idling the thrust even though the head wind is still increasing. Because of the amplitude, duration, and steadiness of the wave, the ground speed decreases from 70 m/s to 44 m/s after 30 sec. As the aircraft enters the head wind to tail wind shear portion of the wave, the airspeed begins to drop and, as the aircraft drops below the glide slope, thrust is increased. However, the ground speed is also beginning to increase due to the tail wind and with the increased thrust, the pilot ends up overcontrolling towards the end of the run. Although this wind field clearly presents no problem with excessive airspeed oscillations and deviation below the glide slope, there is evidence of overcontrol by the control logic gains used to represent the pilot. The set response is too fast for such a long wave and the fixed gains for thrust and elevator control should be readjusted due to the quasi-steadiness and large wave amplitude of the wind field. The airspeed deviation parameters are small relative to the previously mentioned runs. The airspeed ranged between 63 m/s and 84 m/s, angle of attack varied between 2.9° and 8.7°, and thrust varied between idle and 95 percent full forward.

In summary, the four flight path deterioration parameters showed increases with increased wave amplitude at the phugoid frequency. However, in the case of the 2 ω_{ph} wave, the large wind gradient caused the aircraft to approach the stall regime. In the 1/2 ω_{ph} wave overcontrol was observed although it was noted that the airspeed oscillations were small for this case.

4.3.2 1 - Cosine Downbursts

1. 5.15 m/s at ω_{ph}. The flight profile of a B727 flown through a 5.15 m/s 1 - cosine downburst at ω_{ph} is shown in Figure 12a. As the aircraft encounters the down draft, it falls below the glide slope despite nose pitch-up and increased thrust. However, as with the longitudinal wave, a "roller coaster" oscillation was set up in vertical velocity resulting in deviations below the glide slope. It should be noted that the V+ and V- parameter values are lower than those of the 5.15 m/s longitudinal sine wave at ω_{ph}. For this run, angle of attack remained fairly steady (5.0° to 7.4°), pitch varied between 3° and 7°, and airspeed ranged between 67 m/s and 76 m/s.

2. 10.3 m/s at ω_{ph}. The trajectory of the aircraft flown through a 10.3 m/s downburst appears in Figure 12b. Again, the "roller coaster" effect is noted and the aircraft is blown below the glide slope. The deterioration parameters are larger than those of the previous run. The angle of attack varied between 3.8° and 8.0°, pitch angle ranged from 2.8° to 10.8°, and airspeed varied between 65.3 m/s and 78.7 m/s. Thrust setting reached idle and full forward limits.

3. 15.45 m/s at ω_{ph}. In Figure 12c, it can be seen that the 15.45 m/s downburst at the phugoid frequency forces the aircraft farthest below the glide slope. Pitch angle varied between 2.8° and 14.9° and angle of attack varied between 3.4° and 8.7°. Thrust setting ranged between idle and full forward settings and airspeed ranged between 63.0 m/s and 80.1 m/s.

4. 15.45 m/s at 2 ω_{ph}. Figure 14b shows the flight profile of a B727 encountering a 15.45 m/s downburst wave at 2 ω_{ph}. Because this wave is shorter in time duration than that of the phugoid period wave, the

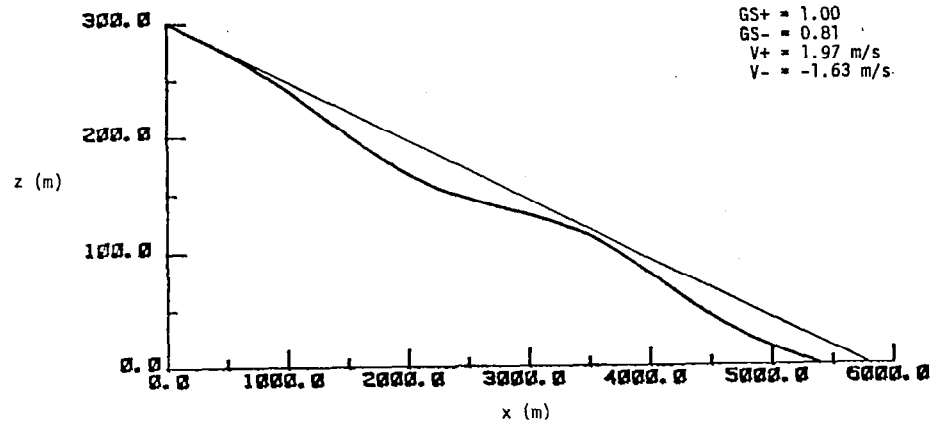

a) Simulated trajectory through a vertical 1 - cosine wave of 5.15 m/s amplitude and ω_{ph} frequency.

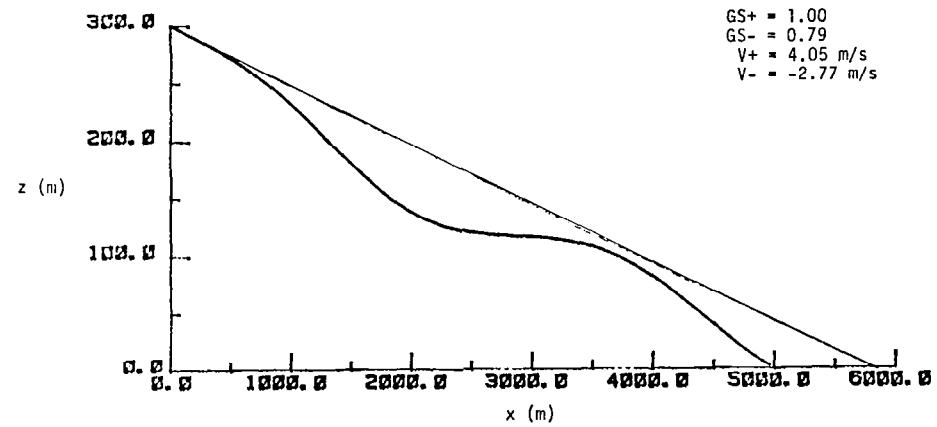

b) Simulated trajectory through a vertical 1 - cosine wave of 10.3 m/s amplitude and ω_{ph} frequency.

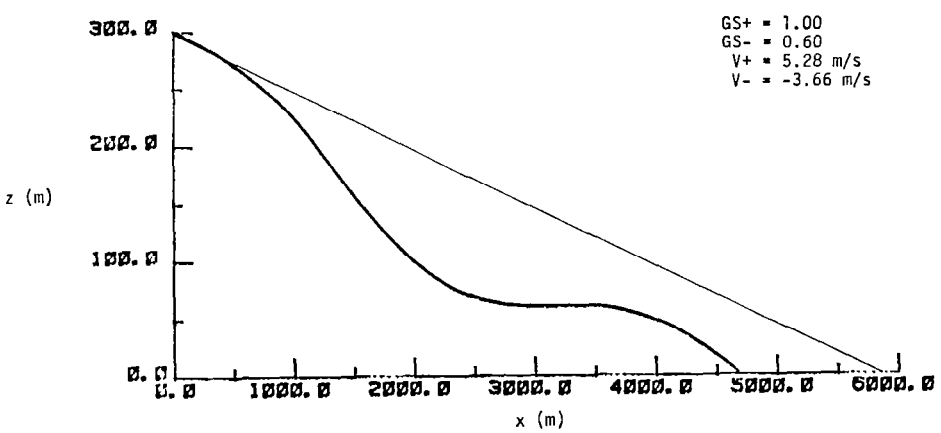

c) Simulated trajectory through a vertical 1 - cosine wave of 15.45 m/s amplitude and ω_{ph} frequency.

Figure 12 Computer-simulated approach trajectory of a B727 using control system II through a vertical 1 - cosine wave downburst.

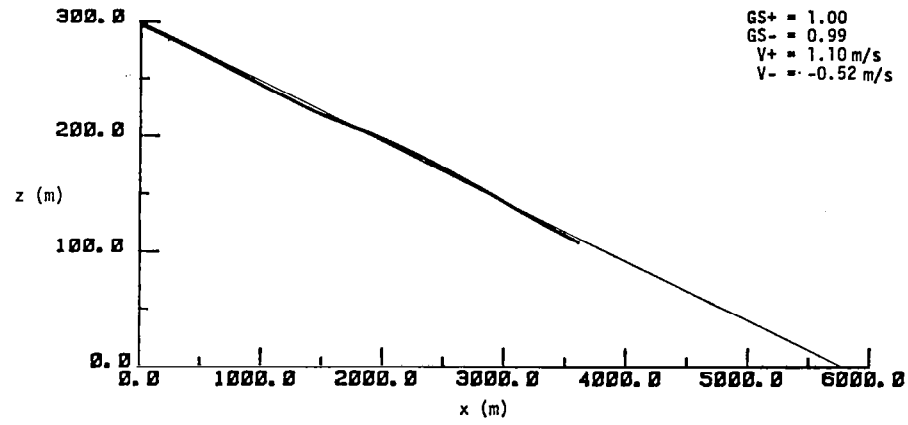

a) Simulated trajectory through a vertical 1 - cosine wave of 5.15 m/s amplitude and ω_{ph} frequency.

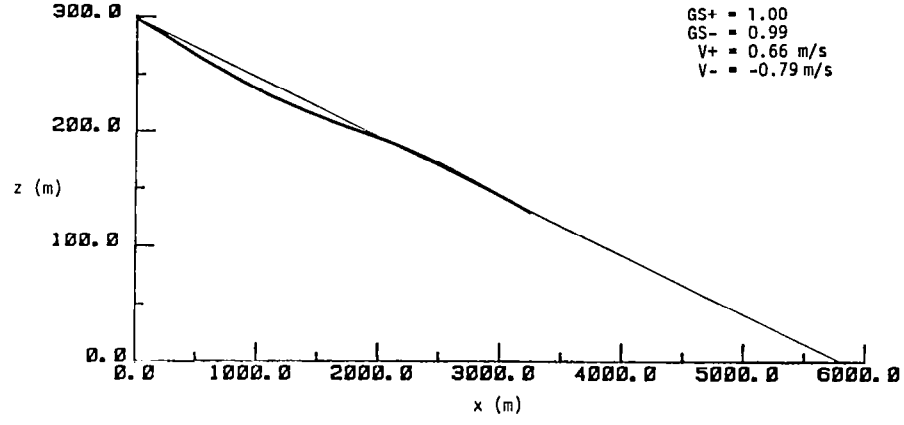

b) Simulated trajectory through a vertical 1 - cosine wave of 10.3 m/s amplitude and ω_{ph} frequency.

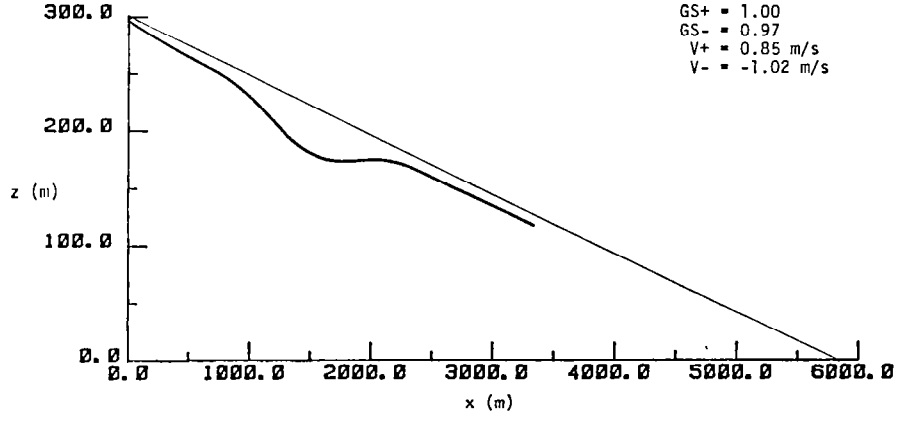

c) Simulated trajectory through a vertical 1 - cosine wave of 15.45 m/s amplitude and ω_{ph} frequency.

Figure 13 Approach trajectory of a B727 aircraft performed by a test pilot in the NASA Ames simulator through a vertical 1 - cosine wave downburst.

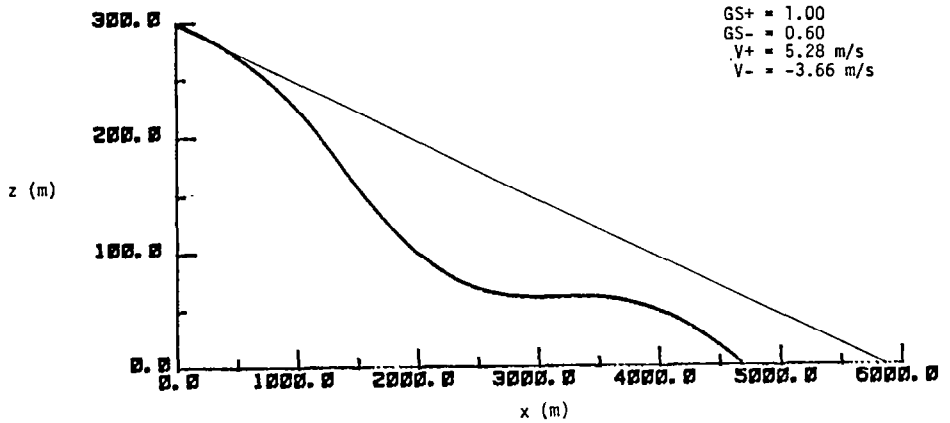

a) Simulated trajectory through a vertical 1 - cosine wave of 15.45 m/s amplitude and ω_{ph} frequency.*

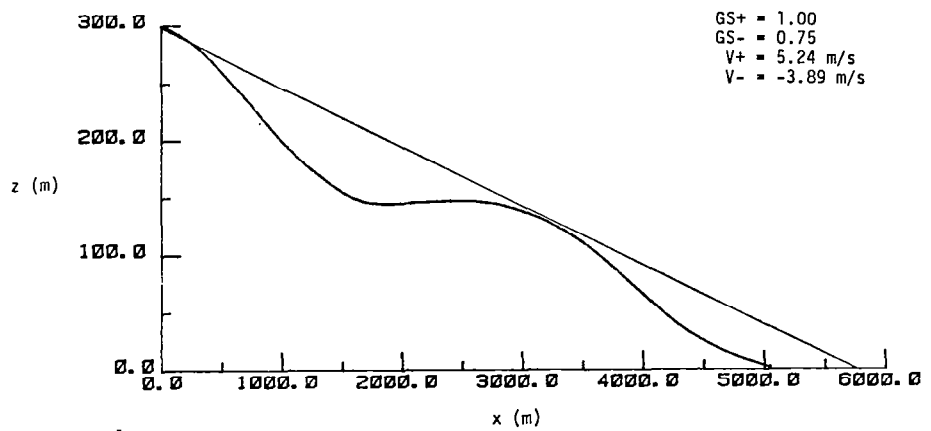

b) Simulated trajectory through a vertical 1 - cosine wave of 15.45 m/s amplitude and 2 ω_{ph} frequency.

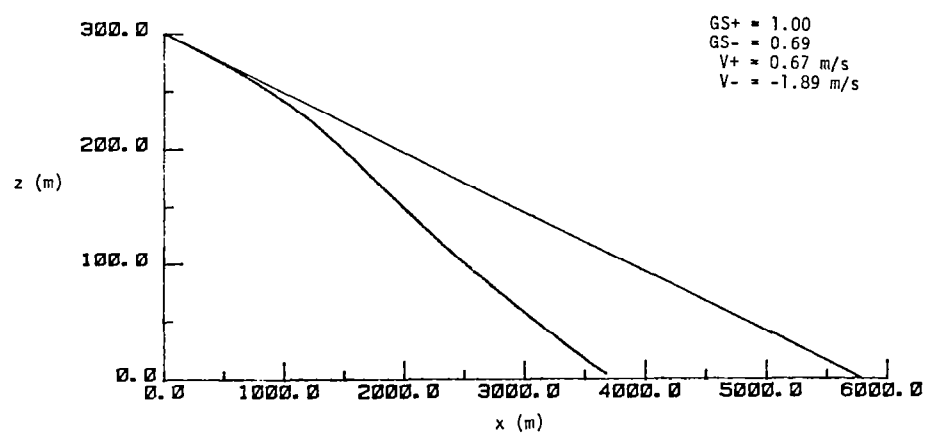

c) Simulated trajectory through a vertical 1 - cosine wave of 15.45 m/s amplitude and 1/2 ω_{ph} frequency.

Figure 14 Computer-simulated approach trajectory of a B727 using control system II through a vertical 1 - cosine wave downburst.

*Repeated from Figure 12 for consistency.

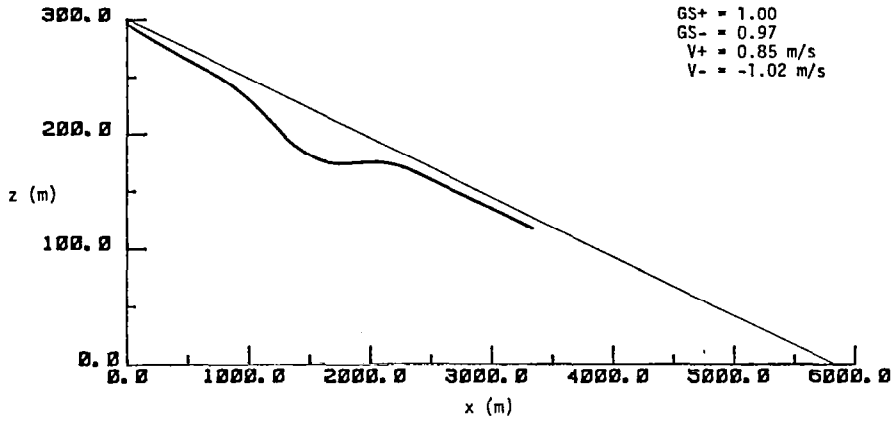

a) Simulated trajectory through a vertical 1 - cosine wave of 15.45 m/s amplitude and ω_{ph} frequency.*

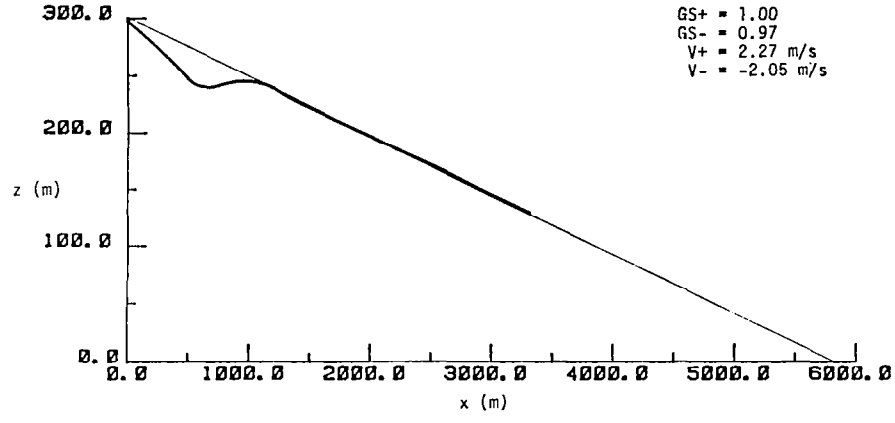

b) Simulated trajectory through a vertical 1 - cosine wave of 15.45 m/s amplitude and 2 ω_{ph} frequency.

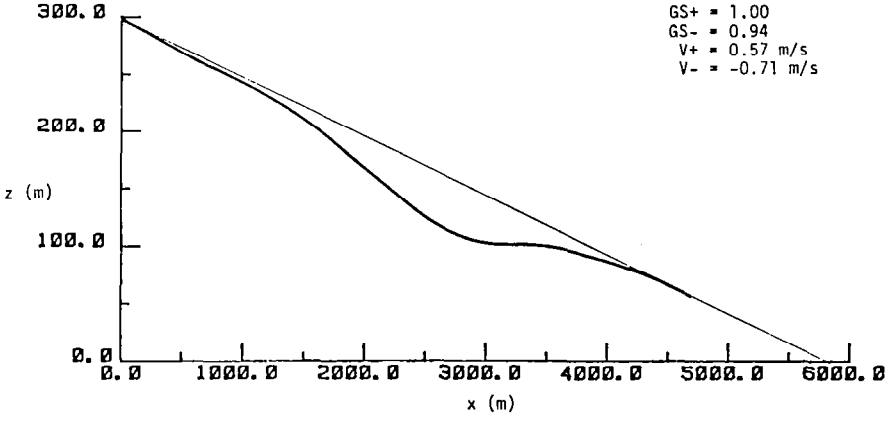

c) Simulated trajectory through a vertical 1 - cosine wave of 15.45 m/s amplitude and 1/2 ω_{ph} frequency.

Figure 15 Approach trajectory of a B727 aircraft performed by a test pilot in the NASA Ames simulator through a vertical 1 - cosine wave wind.

*Repeated from Figure 13 for consistency.

aircraft remains in the down draft for a shorter time and the altitude deviation from the glide slope is not as severe as it was in the phugoid wave. The airspeed deviation parameters are similar to those of the phugoid wave. The pitch angle varied from 2.7° to 16.0° and angle of attack ranged between 3.0° and 10.3°. Airspeed ranged from 60.5 m/s to 81.8 m/s and idle to full throttle limits were reached.

5. 15.45 m/s at 1/2 ω_{ph}. The flight of a B727 through a 15.45 m/s 1 - cosine downburst at 1/2 ω_{ph} is shown in Figure 14c. The magnitude and duration of this wave forces the aircraft below the glide slope and causes premature impact. This is also due to the fact that the aircraft encounters the wave relatively close to the ground. Airspeed deviation is very small as indicated by the low values of V+ and V- and the fact that airspeed varied only between 66.6 m/s and 70.1 m/s. Angle of attack varied between 6.2° and 7.3° and pitch angle varied between 3.3° and 14.6°. Thrust ranged from approach thrust to full forward.

In summary, the flight profile deteriorates with increasing downburst amplitude at the phugoid frequency. However, the worst case occurred not at the phugoid frequency but at the longest wave (1/2 ω_{ph}). Thus it appears that the longer the aircraft is in the downburst, the greater the flight path deterioration.

4.3.3 S-Shape Waves

1. 5.15 m/s at ω_{ph}. Figure 16a shows the simulated trajectory of a B727 through a 5.15 m/s longitudinal S-shape shear wave at ω_{ph}. This wave presents very little problem in flight path and airspeed deviations and is handled well by the pilot. In this run, angle of attack varied between 5.6° and 6.9°, airspeed ranged between 68.3 m/s and 72.1 m/s, and thrust setting varied from 20 percent to 53 percent full power.

2. 10.3 m/s at ω_{ph}. The flight profile through a 10.3 m/s wave at the same frequency is presented in Figure 16b. Although the four deterioration parameters have increased, this wave does not present a serious control problem for the pilot. The angle of attack varied between 5.0° and 7.6°, airspeed deviated between 66.3 m/s and 74.4 m/s, and thrust ranged from idle to 73 percent full power.

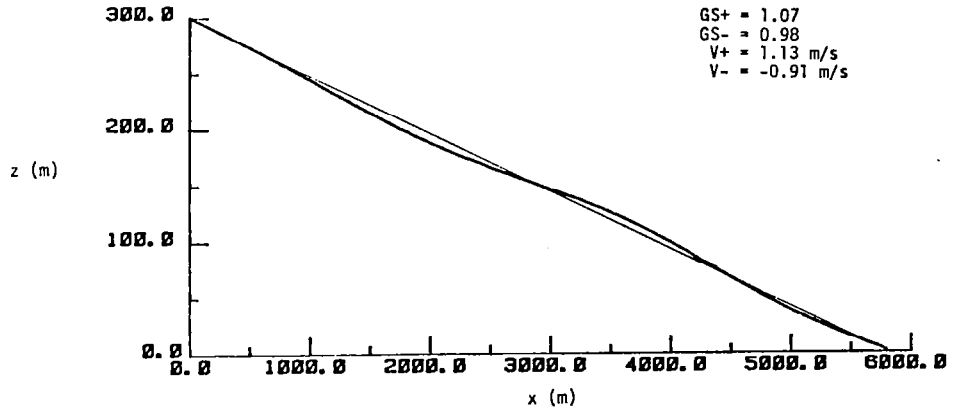

a) Simulated trajectory through a longitudinal S-shape wave of 5.15 m/s amplitude and ω_{ph} frequency.

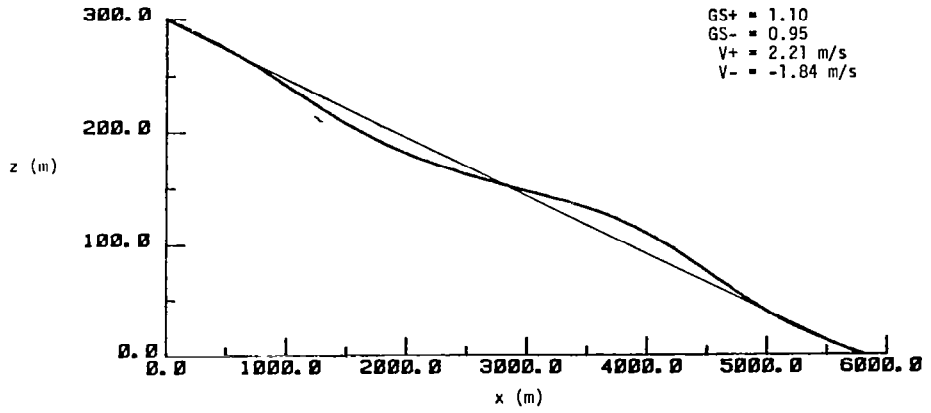

b) Simulated trajectory through a longitudinal S-shape wave of 10.3 m/s amplitude and ω_{ph} frequency.

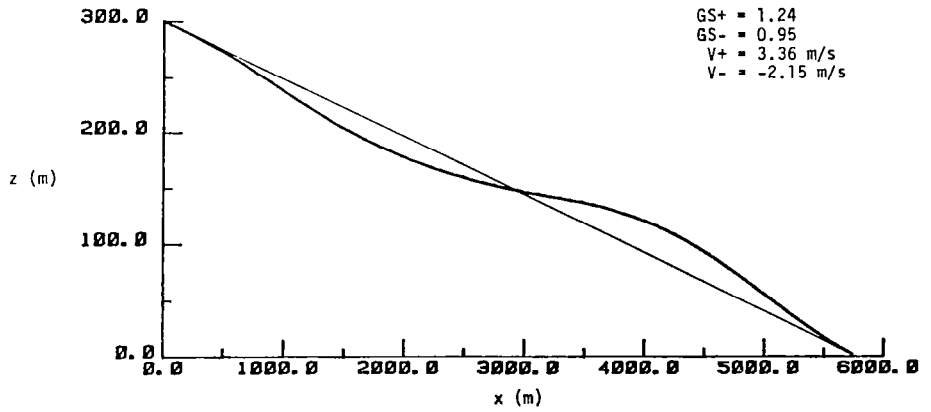

c) Simulated trajectory through a longitudinal S-shape wave of 15.45 m/s amplitude and ω_{ph} frequency.

Figure 16 Computer-simulated approach trajectory of a B727 using control system II through a longitudinal S-shape wave wind.

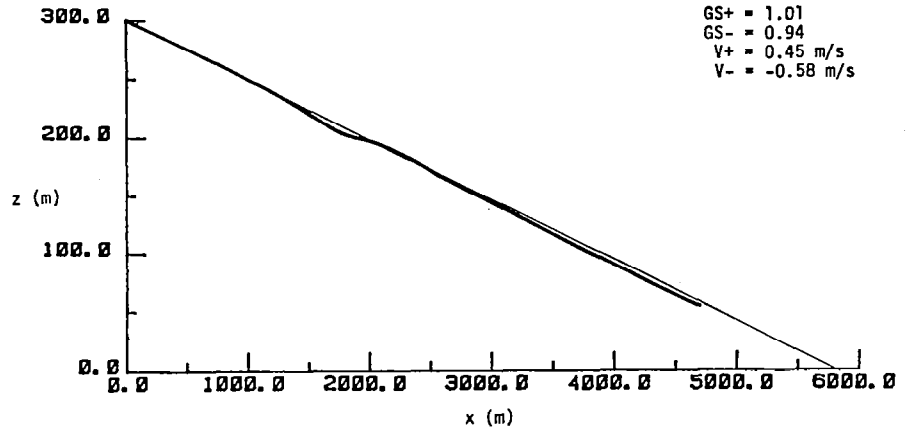

a) Simulated trajectory through a longitudinal S-shape wave of 5.15 m/s amplitude and ω_{ph} frequency.

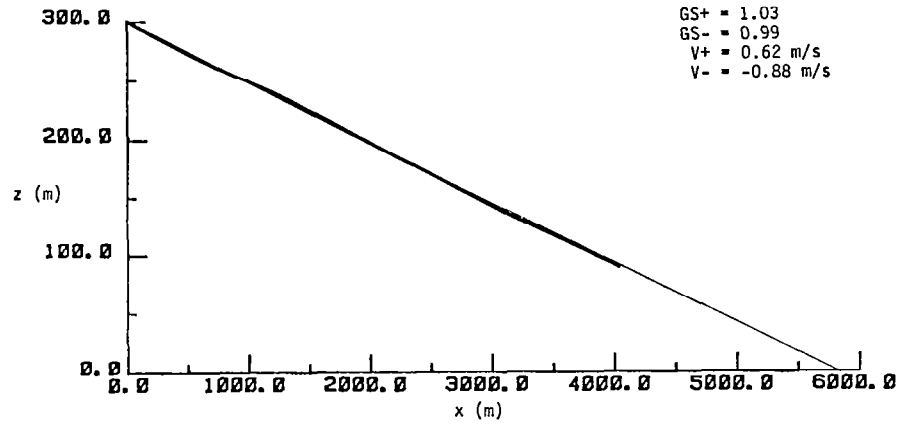

b) Simulated trajectory through a longitudinal S-shape wave of 10.3 m/s amplitude and ω_{ph} frequency.

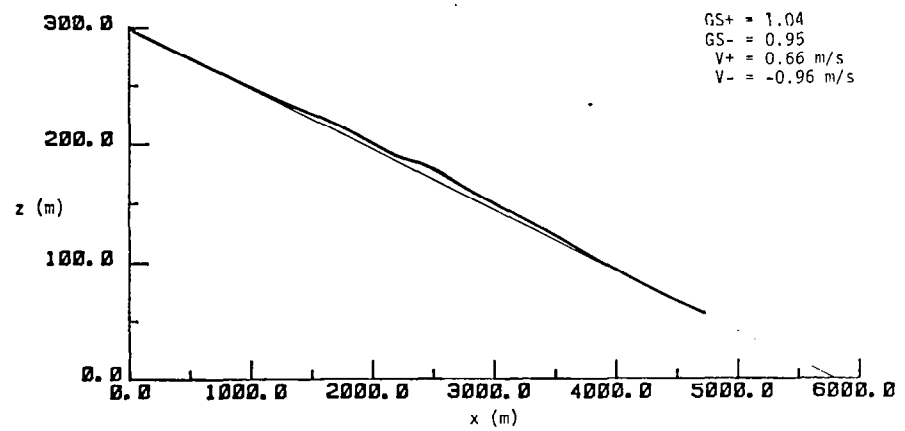

c) Simulated trajectory through a longitudinal S-shape wave of 15.45 m/s amplitude and ω_{ph} frequency.

Figure 17 Approach trajectory of a B727 aircraft performed by a test pilot in the NASA Ames simulator through a longitudinal S-shape wave wind.

3. 15.45 m/s at ω_{ph}. In the case of a 15.45 m/s wave at ω_{ph} (Figure 16c), the deterioration parameters have increased and control is more difficult to attain. Angle of attack was maintained between 4.4° and 8.0° and airspeed ranged between 65.3 m/s and 76.4 m/s. Thrust setting varied from idle to 87 percent full forward.

4. 15.45 m/s at 2 ω_{ph}. Figure 18b shows the flight path of the aircraft flown through a 15.45 m/s S-shape wave at 2 ω_{ph}. It appears that the larger longitudinal wind gradient (due to large wave amplitude and short wavelength) and the pilot's control inputs cause greater airspeed oscillations and a greater drop below the glide slope. In this case, angle of attack varied from 3.1° to 9.0° and airspeed ranged between 62.1 m/s and 81.8 m/s. Idle and full thrust limits were reached.

5. 15.45 m/s at 1/2 ω_{ph}. The aircraft encounter with the 15.45 m/s wave at 1/2 ω_{ph} caused little airspeed and flight path deviation. The slight overcontrol tendencies of the pilot control system logic due to the fixed gains and the long wave duration can be noted near the end of the trajectory (Figure 18c). The airspeed oscillated between 69.2 m/s and 71.4 m/s and angle of attack was maintained between 5.8° and 6.5°. Thrust ranged between 27 percent and 55 percent full forward.

In summary, the flight profiles deteriorated with increasing wave amplitude at the phugoid frequency. However, the effects of the large wind gradient caused the largest deterioration in the case of the 2 ω_{ph} wave at 15.45 m/s amplitude. The 1/2 ω_{ph} was seen to cause no serious control problems.

4.3.4 Combination S-Shape Waves and Downbursts

The previously mentioned longitudinal S-shape and sine waves and vertical downburst profiles were examined individually to determine the aircraft/pilot response to that particular wind component. The next four cases were run to examine the combined effects of longitudinal S-shape waves and 1 - cosine downbursts. This combined profile is the most realistic with respect to the actual thunderstorm downburst cell wind field. Fujita and Caracena's analysis [2] of the Eastern 66 accident in Figure 20 shows the downburst cell located along the aircraft's approach

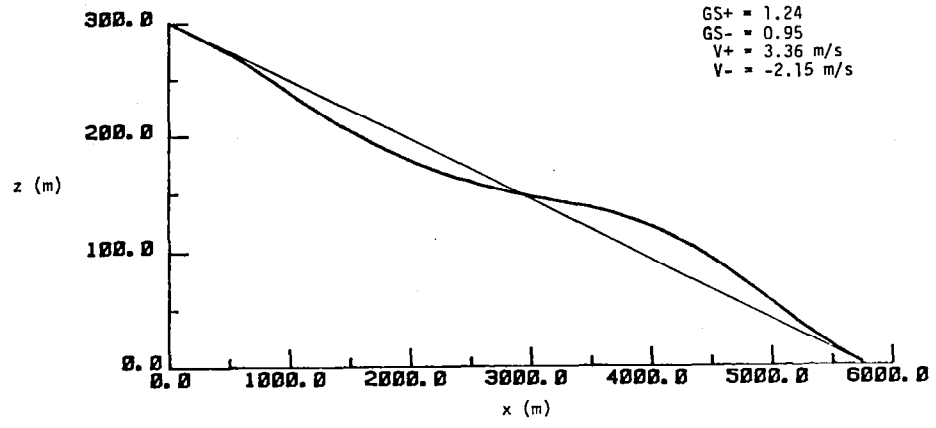

a) Simulated trajectory through a longitudinal S-shape wave of 15.45 m/s amplitude and ω_{ph} frequency.*

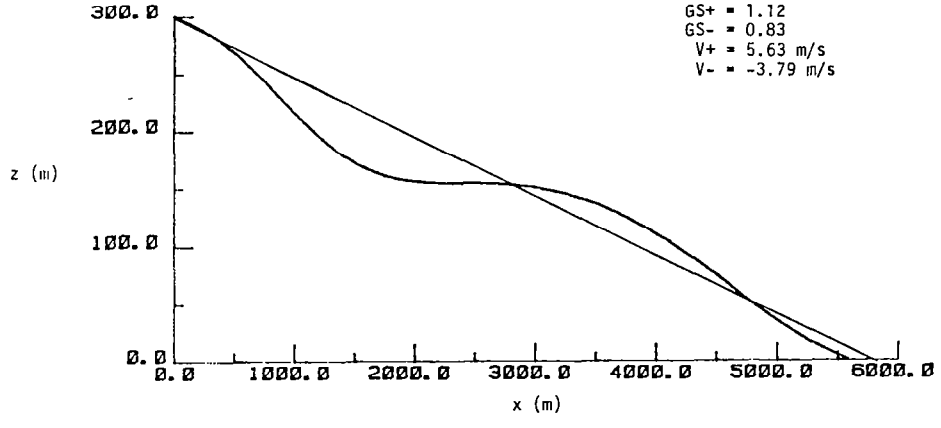

b) Simulated trajectory through a longitudinal S-shape wave of 15.45 m/s amplitude and 2 ω_{ph} frequency.

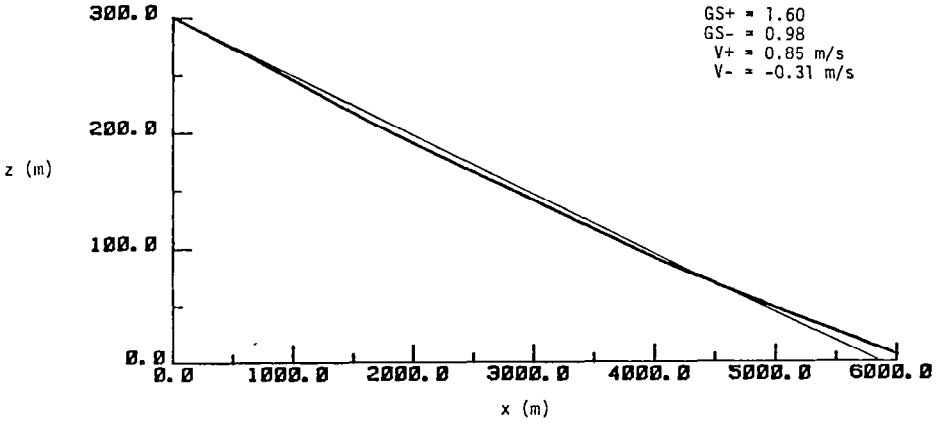

c) Simulated trajectory through a longitudinal S-shape wave of 15.45 m/s amplitude and 1/2 ω_{ph} frequency.

Figure 18 Computer-simulated approach trajectory of a B727 using control system II through a longitudinal S-shape wave wind.

*Repeated from Figure 16 for consistency.

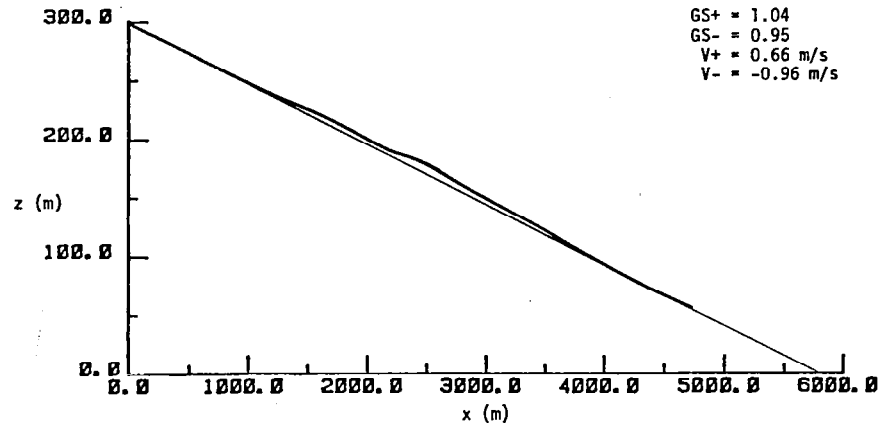

a) Simulated trajectory through a longitudinal S-shape wave of 15.45 m/s amplitude and ω_{ph} frequency.*

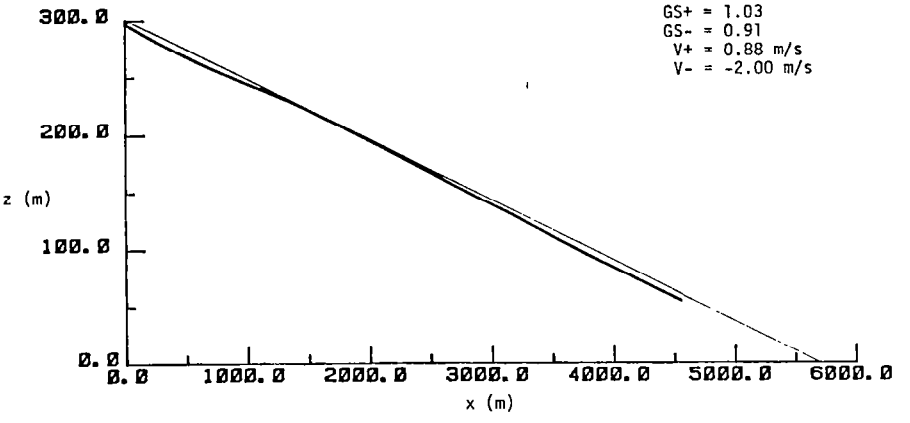

b) Simulated trajectory through a longitudinal S-shape wave of 15.45 m/s amplitude and 2 ω_{ph} frequency.

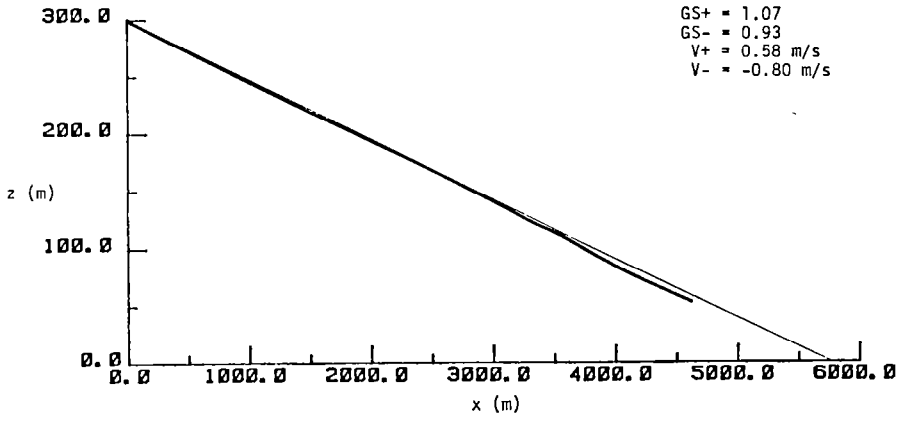

c) Simulated trajectory through a longitudinal S-shape wave of 15.45 m/s amplitude and 1/2 ω_{ph} frequency.

Figure 19 Approach trajectory of a B727 aircraft performed by a test pilot in the NASA Ames simulator through a longitudinal S-shape wave wind.

*Repeated from Figure 17 for consistency.

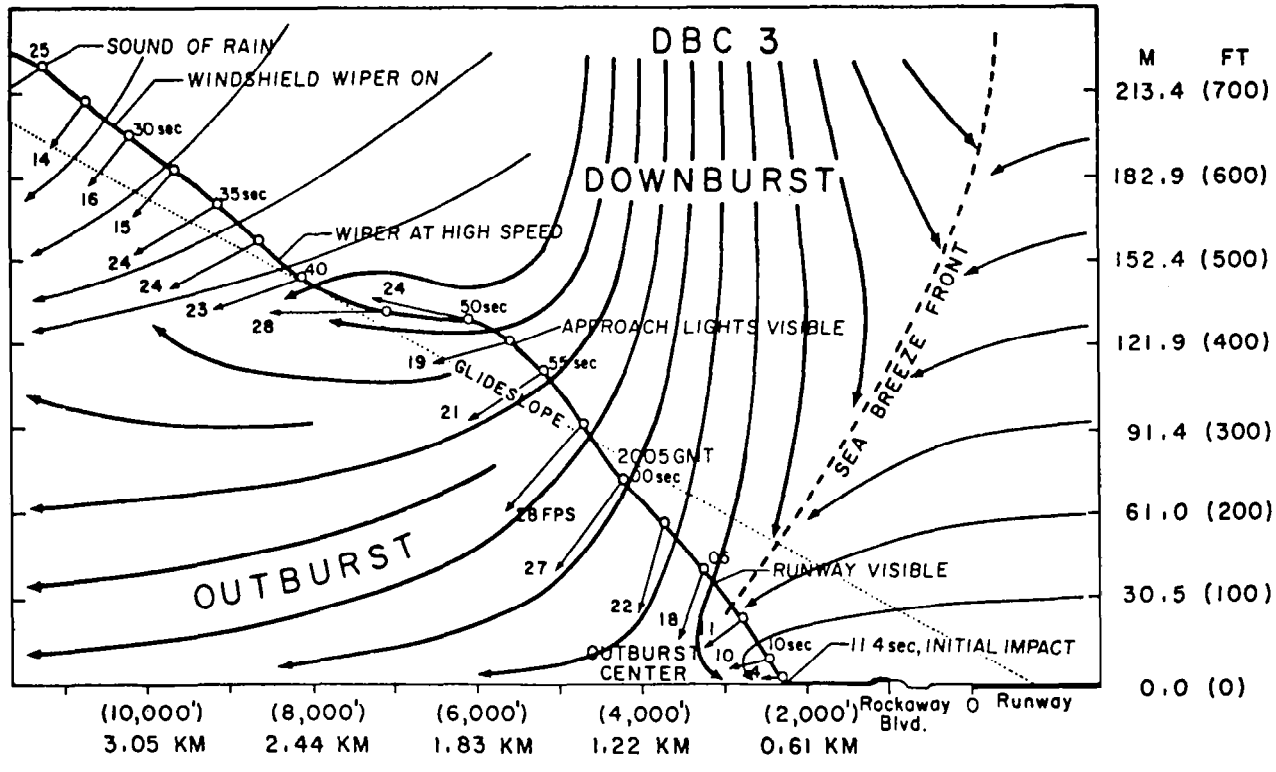

Figure 20 The flight path of Eastern 66 and associated wind field as analyzed by Fujita and Caracena [2].

path. As the downburst reaches the ground, it spreads out. The aircraft encounters a head wind to tail wind shear causing airspeed loss and a strong down draft causing descent below the glide slope. Thus, the combined effects of the longitudinal and vertical winds in the thunderstorm downburst cell present a serious hazard to an aircraft operating at low altitude.

1. 5.15 m/s at ω_{ph}. A comparison between Figure 12a (5.15 m/s downburst at ω_{ph}) and Figure 21 (combination of downburst and S-shape wave) reveal little difference in flight path deterioration. Angle of attack varied between 4.6° and 7.6° and airspeed varied between 66.2 m/s and 75.4 m/s. Thrust setting ranged between idle and 75 percent full forward power.

2. 10.3 m/s at ω_{ph}. Comparison of Figure 12b (10.3 m/s downburst at ω_{ph}) and Figure 22a (combination of downburst and S-shape wave) also shows little difference in flight path deterioration. This reveals that the smaller amplitude 5.15 m/s and 10.3 m/s S-shape waves, which were shown to have little effect by themselves, cause no additional difficulty when acting in conjunction with the smaller amplitude downburst waves.

3. 20.6 m/s at ω_{ph}. The combined airspeed loss due to a 20.6 m/s S-shape longitudinal wave and vertical velocity increase due to a 20.6 m/s 1 - cosine downburst at ω_{ph} forced the aircraft to descend below the glide slope and impact prematurely (Figure 22b). The large value of V- indicates a large drop in airspeed below the approach airspeed. The airspeed in this case decreased to a minimum of 54.3 m/s and the angle of attack reached 13.2°.

4. 20.6 m/s at 2 ω_{ph}. Figure 22c shows the trajectory for the 2 ω_{ph} case. The large wind gradients and combined effects of the S-shape wave and downburst caused the aircraft to descend below the glide slope. In this case, the airspeed dropped to 49.8 m/s and the angle of attack entered the stall regime (approximately 16°) resulting in a loss of control. The large value of airspeed warning parameter V- indicates a large airspeed drop below the approach value and would warn the pilot of the possibility of a stall.

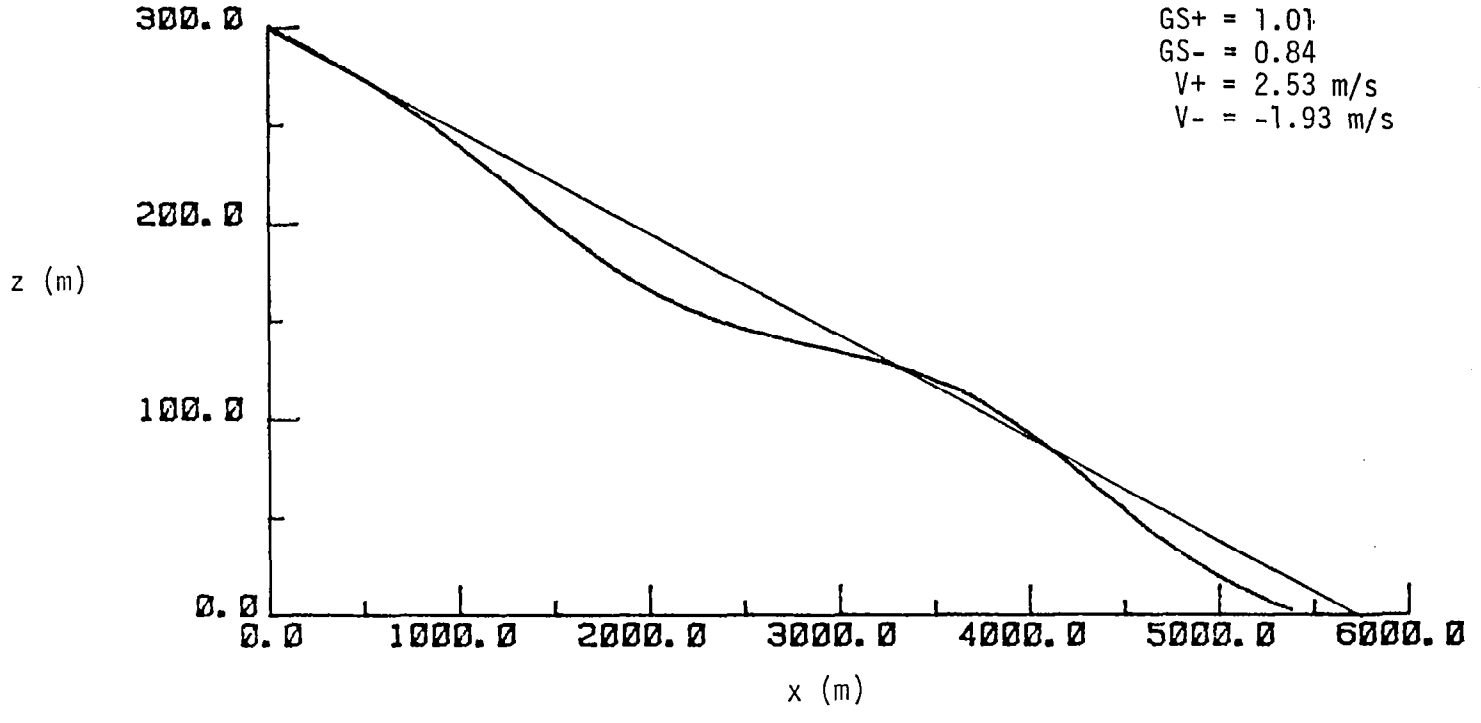

Simulated trajectory through a combination longitudinal S-shape and vertical 1 - cosine wave of 5.15 m/s amplitude and ω_{ph} frequency.

Figure 21 Computer-simulated approach trajectory of a B727 using control system II through a combination longitudinal S-shape and vertical 1 - cosine wave wind.

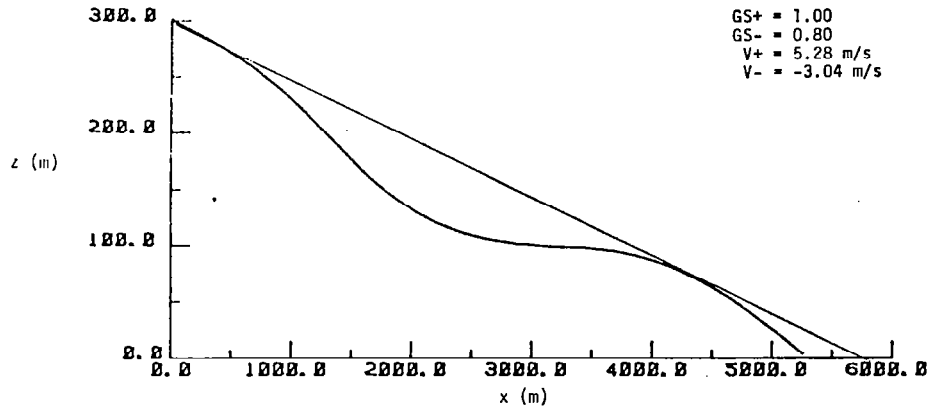

a) Simulated trajectory through a combination longitudinal S-shape and vertical 1 - cosine wave of 10.3 m/s amplitude and ω_{ph} frequency.

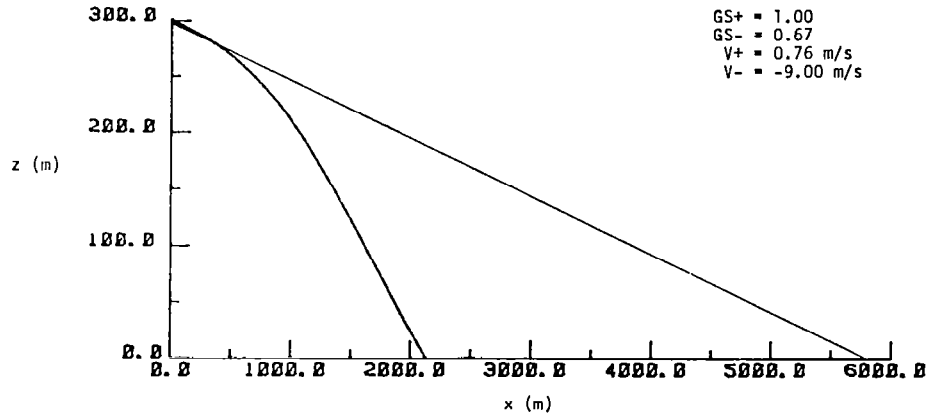

b) Simulated trajectory through a combination longitudinal S-shape and vertical 1 - cosine wave of 20.6 m/s amplitude and ω_{ph} frequency.

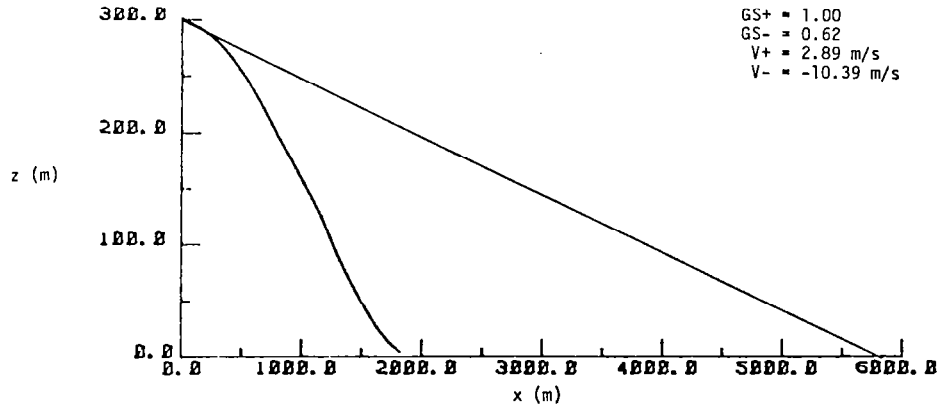

c) Simulated trajectory through a combination longitudinal S-shape and vertical 1 - cosine wave of 20.6 m/s amplitude and 2 ω_{ph} frequency.

Figure 22 Computer-simulated approach trajectory of a B727 using control system II through a combination longitudinal S-shape and vertical 1 - cosine wave wind.

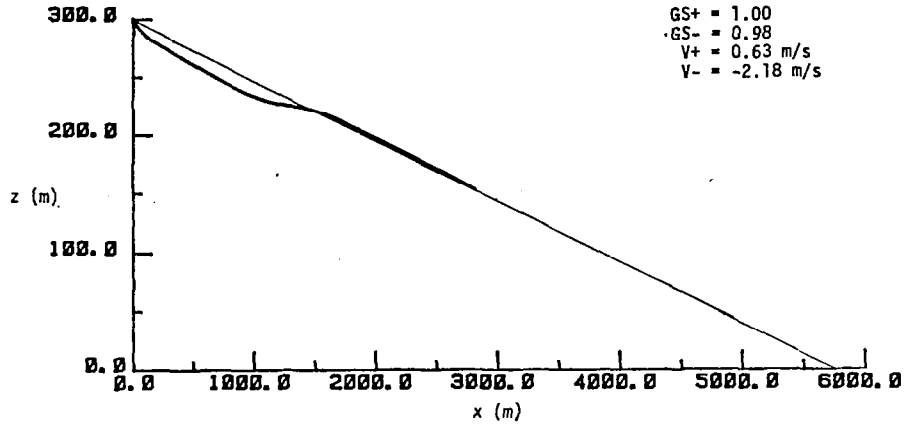

a) Simulated trajectory through a combination longitudinal S-shape and vertical 1 - cosine wave of 10.3 m/s amplitude and ω_{ph} frequency.

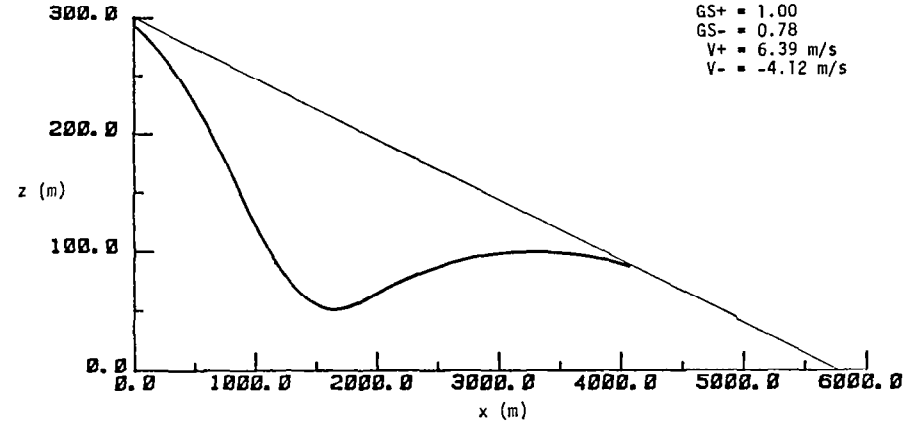

b) Simulated trajectory through a combination longitudinal S-shape and vertical 1 - cosine wave of 20.6 m/s amplitude and ω_{ph} frequency.

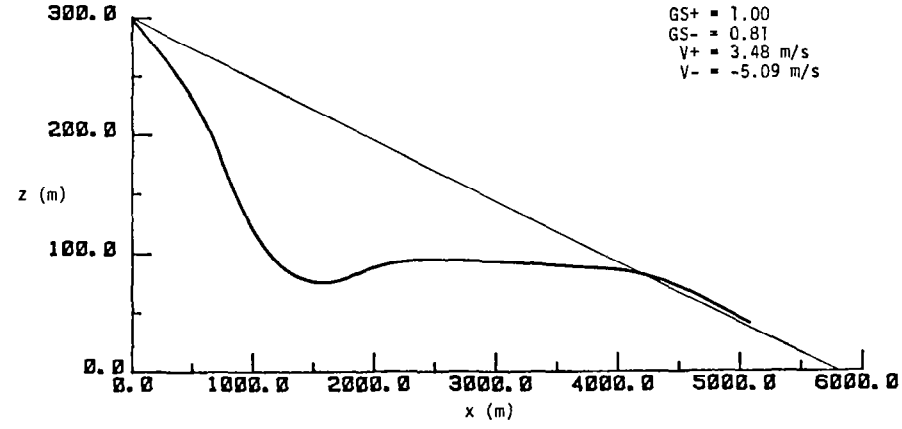

c) Simulated trajectory through a combination longitudinal S-shape and vertical 1 - cosine wave of 20.6 m/s amplitude and 2 ω_{ph} frequency.

Figure 23 Approach trajectory of a B727 aircraft performed by a test pilot in the NASA Ames simulator through a combination longitudinal S-shape and vertical 1 - cosine wave wind.

Finally, in Figure 24 a test run was made through a 15.45 m/s sine wave at ω_{ph} using the pilot control system logic III as discussed in Section 2.3. This system controls airspeed by throttle rate control and pitch attitude and touchdown point by elevator control. Comparison with the flight path deterioration parameters in Figure 8c reveals that this pilot control model does not allow the aircraft to sink as far below the glide slope. Additionally, the airspeed deterioration parameters V+ and V- are reduced. However, a relatively high vertical velocity is needed to bring the aircraft to the touchdown point due to a rise above the glide slope at a relatively low altitude.

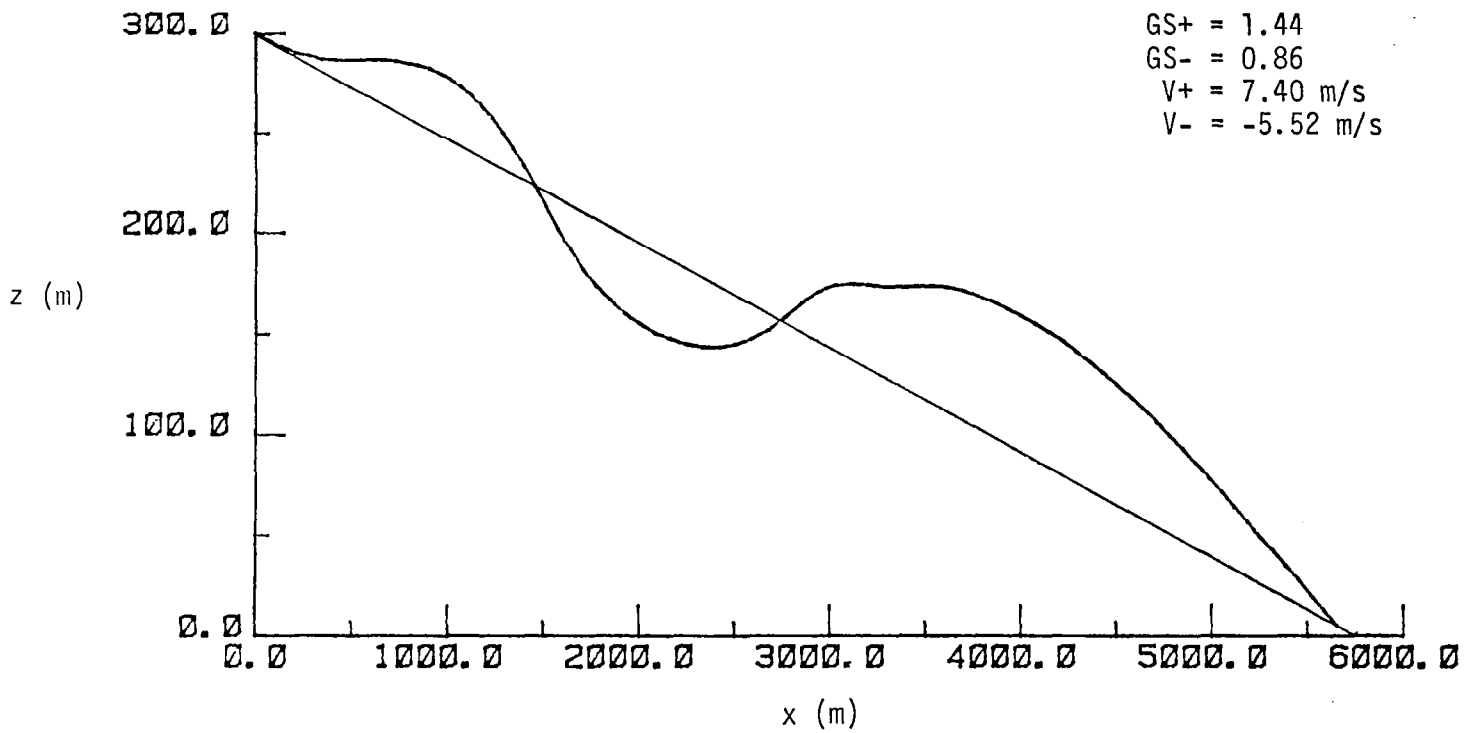

Figure 24 Computer-simulated approach trajectory of a B727 using control system III through a longitudinal sine wave wind of 15.45 m/s amplitude and ω_{ph} frequency.

CHAPTER 5. DESCRIPTION OF FLIGHT SIMULATOR TESTS CONDUCTED AT NASA AMES

5.1 Flight Simulator Results

The following tests corresponding to the test plan described in Table 1 were run in the B727 flight simulator at NASA Ames. The profiles were flown by a test pilot for the purpose of evaluating the response of the aircraft/pilot system to various thunderstorm environment wind shears.

5.1.1 Sine Waves (Figures 9 and 11)

1. 5.15 m/s at ω_{ph}. This run did not cause serious control difficulty for the pilot. The pilot decreased thrust and pitched nose down when encountering the increasing head wind portion of the wave. As the head wind sheared to a tail wind, the pilot pitched nose up and increased thrust. The pilot maintained better airspeed control (67.0 m/s to 74.2 m/s) as compared with 63.7 m/s to 81.2 m/s in the computer simulation. Flight path angle and angle of attack were also kept within closer constraints. Thrust control ranged from idle to 88 percent power compared to idle and 83 percent in the computer model.

2. 10.3 m/s at ω_{ph}. This simulation presented a greater control problem than the previous run. The flight path and pitch angle variations were larger than those of the previous run and angle of attack ranged from 2.5° to 10.5° as compared with 1.8° and 10.0° for the computer simulation. Airspeed varied from 58.8 m/s to 77.3 m/s (59.8 m/s to 89.6 m/s for computer model) and thrust ranged from idle to full as in the computer run.

3. 15.45 m/s at ω_{ph}. This simulation was similar in control difficulty to the 10.3 m/s run. This is probably a result of the pilot learning from the preceding simulations. The airspeed was maintained between 61.3 m/s and 85.0 m/s as compared to 56.9 m/s and 93.8 m/s in the computer run. Near idle to full forward thrust limits were reached.

4. 20.6 m/s at ω_{ph}. In this run, the pilot showed further evidence of "learning" since the wave frequency had been kept the same as for the previous runs. However, greater thrust and elevator control were needed to maintain the flight path. The pilot kept airspeed between 61.9 m/s and 89.6 m/s compared with 54.4 m/s and 97.0 m/s in the computer simulation. Angle of attack reached 8.2° compared with 12.6° in the computer simulation.

5. 20.6 m/s at 2 ω_{ph}. This profile took the pilot by surprise and, as in the computer simulation, aircraft control was lost. However, the test pilot was able to recover before landing but not without significant altitude and flight path angle deviations. Angle of attack reached 18.5° (stall regime) as in the computer model. Airspeed fell to 50.0 m/s (45.4 m/s in simulation). This simulation agrees well with the computer model and suggests that large wind gradients due to large wave amplitude and short wavelength may seriously affect aircraft operations. The effects of large amplitude at frequencies within some bandwidth of the phugoid frequency must be further examined.

6. 20.6 m/s at 1/2 ω_{ph}. This wave presented no difficulty with regard to flight path angle and deviation below the glide slope. Airspeed was kept between 64.9 m/s and 85.6 m/s (63.0 m/s and 84.0 m/s for computer run). However, tighter pitch and angle of attack control by the test pilot than by the simulated pilot made the difference in more accurate flight path control. It was noted that the computer-simulated pilot tended to overcontrol near the termination of the run and was therefore not an accurate representation of pilot performance in a large amplitude, long wavelength shear.

5.1.2 1 - Cosine Downbursts (Figures 13 and 15)

1. 5.15 m/s at ω_{ph}. Flight through this profile caused slight flight path angle deviations. The pilot pitched nose up to a maximum of 7° (7° in computer simulation) and increased thrust during the downburst encounter. Angle of attack remained fairly constant between 4.2° and 6.4° compared with the model's 5.0° and 7.4°. Airspeed varied from 67.0 m/s to 71.1 m/s compared to 67.0 m/s to 74.0 m/s for the model.

2. 10.3 m/s at ω_{ph}. Larger pitch and thrust were needed to control the flight path angle in this profile. Pitch ranged between 2.5° to 11.0° (compared with the simulation's 2.8° to 10.8°) and maximum angle of attack reached 6.3° compared with 8.0° for the model. Airspeed varied from 66.5 m/s to 70.0 m/s (model, 65.3 m/s to 78.7 m/s). The test pilot performed better on this run than the simulated pilot.

3. 15.45 m/s at ω_{ph}. Large flight path angle and significant altitude deviations occurred during this run. The pilot had to make large pitch and thrust corrections to readjust and maintain the approach. A maximum pitch angle of 13.0° was reached (14.9° for computer model) and maximum angle of attack reached 7.4° (8.7° for computer simulation). However, airspeed and thrust were more accurately controlled by the test pilot than by the simulated pilot and he was therefore able to recover where the computer model could not.

4. 15.45 m/s at 2 ω_{ph}. As in the computer simulation, the test pilot has less difficulty with this downburst wave than with the 1/2 ω_{ph} wave. Large flight path and altitude deviations occurred over the 19 sec duration of the wave and large thrust and pitch inputs were needed to restabilize the approach. Maximum angle of attack reached 9.3° (10.3° for model) and airspeed varied from 64.4 m/s to 74.7 m/s (model, 60.5 m/s to 81.8 m/s).

5. 15.45 m/s at 1/2 ω_{ph}. As in the computer simulation, the test pilot had the greatest difficulty with this profile. The test pilot was better able to negotiate this downburst but not without large thrust and pitch activity (14.5° maximum, 14.6° for model). The test pilot was able to keep airspeed between 67.0 m/s and 70.1 m/s and angle of attack nearly constant at 5.0°. However, large flight path angle and altitude deviations occurred before the aircraft was restabilized.

5.1.3 S-Shape Waves (Figures 17 and 19)

1. 5.15 m/s at ω_{ph}. The pilot encountered little difficulty with this profile. The computer model also experienced little difficulty. Airspeed varied from 67.0 m/s to 70.1 m/s compared with 68.3 m/s and 72.1 m/s for the model.

2. 10.3 m/s at ω_{ph}. This profile also presented no problem for the test pilot. As airspeed decreased due to the head wind to tail wind shear, thrust was increased and then decreased when the aircraft was retrimmed for the remaining tail wind. Airspeed was held between 67.0 m/s and 70.6 m/s compared with 66.3 m/s and 74.4 m/s for the model. The test pilot flew better than the model pilot because of better airspeed/thrust management.

3. 15.45 m/s at ω_{ph}. The pilot had little problem with this S-shape wave while the simulated pilot experienced larger airspeed and altitude deviations. Despite the fact that the test pilot has thus far flown more precisely than the model pilot, the precision of this approach may also be due to "learning." Airspeed ranged between 66.5 m/s and 70.6 m/s compared with 65.3 m/s and 76.4 m/s for the model. Flight path, pitch, and angle of attack were kept nearly constant.

4. 15.45 m/s at 2 ω_{ph}. This shear wave required a large thrust input over a short time period by the pilot. The maximum angle of attack was 8.2° (9.0° for the model) and airspeed ranged between 62.4 m/s and 72.0 m/s compared with 62.1 m/s and 81.8 m/s for the model. Although the test pilot flew this approach better than the model pilot due to better thrust/airspeed control, this case presented the greatest control problem for both. This supports the reasoning that large wave amplitudes at frequencies within some bandwidth bracketing the phugoid frequency may cause hazardous airspeed and altitude deviations.

5. 15.45 m/s at 1/2 ω_{ph}. This profile required very little thrust and pitch input from the test pilot as with the simulated pilot. Airspeed varied from 67.5 m/s to 70.4 m/s compared with 69.2 m/s and 71.4 m/s for the model. Flight path, pitch, and angle of attack were closely maintained by the test pilot and the model, although the test pilot again flew a more precise approach.

5.1.4 Combination S-Shape Waves and Downbursts (Figure 23)

1. 5.15 m/s at ω_{ph}. The test pilot encountered little difficulty with this profile. When the downburst and longitudinal shear were encountered, the pilot increased pitch attitude and thrust to maintain

approach. This profile did not cause very significant problems for the computer simulation although the test pilot flew it more precisely.

2. 10.3 m/s at ω_{ph}. This profile required larger pitch (12.5°) and thrust changes by the test pilot. Some altitude and flight path angle deviations occurred and a relatively safe approach was made again with greater precision than that of the simulated pilot.

3. 20.6 m/s at ω_{ph}. As in the computer model, this profile caused very large altitude and flight path angle deviations. The test pilot stated that the simulated aircraft had been "forced significantly below the glide slope" before he was able to barely recover. Airspeed reached a minimum of 57.4 m/s compared with 54.3 m/s for the model and maximum angle of attack reached 13.2° (13.2° for the model).

4. 20.6 m/s at 2 ω_{ph}. This profile caused loss of control as did the previous case. Again significant flight path angle, airspeed, and altitude deviations occurred resulting in a loss of control. This was shown to occur in the computer simulation as well. Airspeed reached a minimum of 50.8 m/s (49.8 m/s for the model) and the angle of attack reached a maximum of 19.1°. However, the test pilot eventually managed to bring the aircraft under control.

5.2 Comparisons Between Computer Results and Simulator Results

The trajectory program was tested for sine wave and S-shape longitudinal shear waves, 1 - cosine downbursts and combinations of longitudinal and vertical waves. The results of these simulations were compared to simulations through the same wind fields flown in the NASA Ames simulator by a test pilot. In terms of aircraft/pilot response, the computer model compared well with the simulator for the sine waves, S-shape waves, downbursts, and combinations. However, some discrepancies existed with regard to the degree of flight path and airspeed control between the computer model and the test pilot. Although the control logic for the model pilot is similar to the control strategy of the test pilot, the test pilot flew consistently better than the model pilot. This is due to the fixed gain structure of the computer model pilot.

The fixed gains for elevator and thrust control were selected as reasonable control responses to airspeed, flight path angle, and pitch attitude variations. A real pilot does not behave in such a rigid manner. In reality, a pilot acts in a variable gain decision-making process which is probably not adequately included in the simplified model. This fixed gain structure of the model allows for lower pilot damping of the flight path and airspeed oscillations induced by encounter with wave disturbances. The test pilot is clearly of better skill than the computer model pilot. In addition, the test pilot had the opportunity to "learn" the types of profiles he was flying during the tests.

The airspeed deterioration parameters calculated for the fixed-stick cases presented earlier in Figure 6 showed that the V+ and V- values for the small amplitude wave (5.15 m/s) at the phugoid frequency were larger than those of the 2 ω_{ph} and 1/2 ω_{ph} waves at the same amplitude. A small amplitude wave was used for the illustration since the aircraft could not handle waves of larger amplitudes in the fixed-stick mode. However, in the cases of large amplitude waves and pilot control, the computer and simulator runs showed that the large amplitude 15.45 m/s S-shape and 20.6 m/s sine waves at 2 ω_{ph} presented the greatest control difficulty for the aircraft/pilot system. The airspeed deterioration parameters V+ and V- calculated from the computer simulations (Figures 25 and 26) are shown to increase with increasing longitudinal wave amplitude for waves at the phugoid frequency. The largest V- values were attained for the 2 ω_{ph} waves. However, the V+ value of the 20.6 m/s sine wave at 2 ω_{ph} is not as large as that of the phugoid frequency wave, which is misleading. The values of V+ and V- from the computer simulations were smallest for the 1/2 ω_{ph} S-shape and sine waves. In comparison with the computer results, similar trends can be noted from the airspeed deterioration parameters from the simulator runs for the S-shape waves and for V+ values of the sine waves. However, in the case of the sine waves, the simulator values of V- tend to be misleading due to the pilot "learning" the profiles and "fine tuning" his control procedures.

Control difficulty was encountered by the computer model and test pilot in flight through downbursts (particularly the 1/2 ω_{ph} wave) and

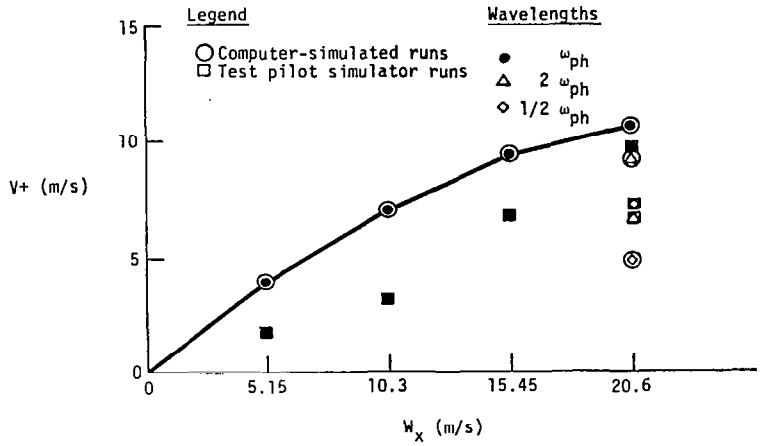

a) V+ values versus sine wave amplitude and frequency.

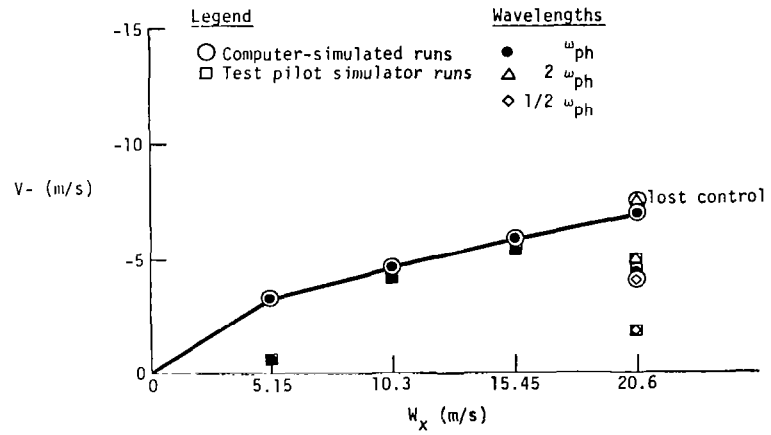

b) V- values versus sine wave amplitude and frequency.

Figure 25 Airspeed deviation parameters for longitudinal sine wave winds.

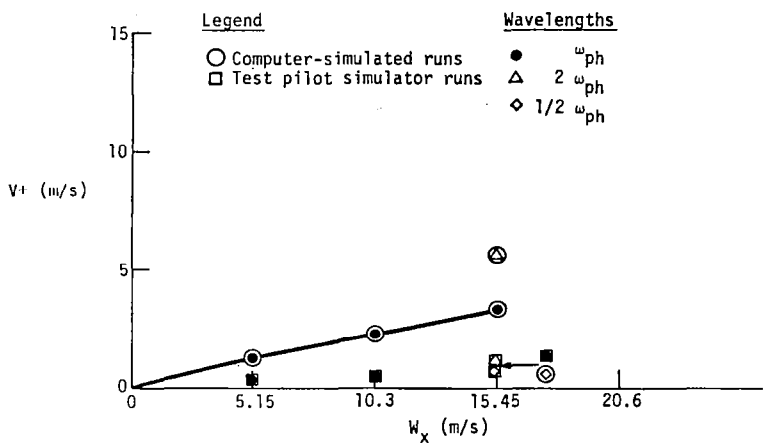

a) V+ values versus S-shape wave amplitude and frequency.

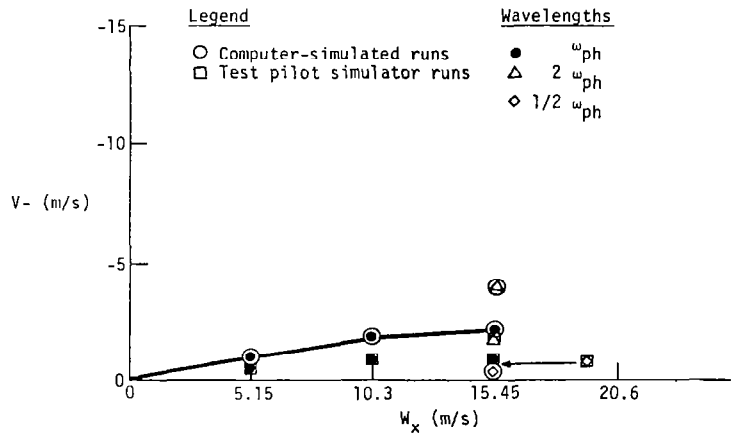

a) V- values versus S-shape wave amplitude and frequency.

Figure 26 Airspeed deviation parameters for longitudinal S-shape wave winds.

in the combination S-shape longitudinal waves and 1 - cosine downbursts. For the downbursts, the computer-generated and simulator airspeed deterioration parameters (Figure 27) were lowest for the 1/2 ω_{ph} wave which caused the largest flight path deviation. This is reasonable since the long wave downburst does not have a pronounced effect on airspeed deviation but instead causes the aircraft to descend below the glide slope with the steadily descending air mass. The aircraft remains in this long wave for 76 seconds. Therefore, airspeed deterioration is probably not a meaningful warning parameter for application to downbursts. It may be noted that the glide slope deviation parameter GS- (Tables 2 and 3) for downbursts show low values corresponding to large descent below the glide slope for the 1/2 ω_{ph} waves and that this type of warning parameter might be more meaningful.

For the combination S-shape longitudinal waves and 1 - cosine downbursts, the decreasing airspeed and the descending air mass forcing the aircraft below the glide slope presented the most difficulty for the simulated pilot and test pilot. The V+ values given in Figure 28a show a misleading trend. However, Figure 28b shows that the largest V- values for airspeed deviation correspond to the worst control cases and would therefore provide a meaningful warning of hazardous wind conditions.

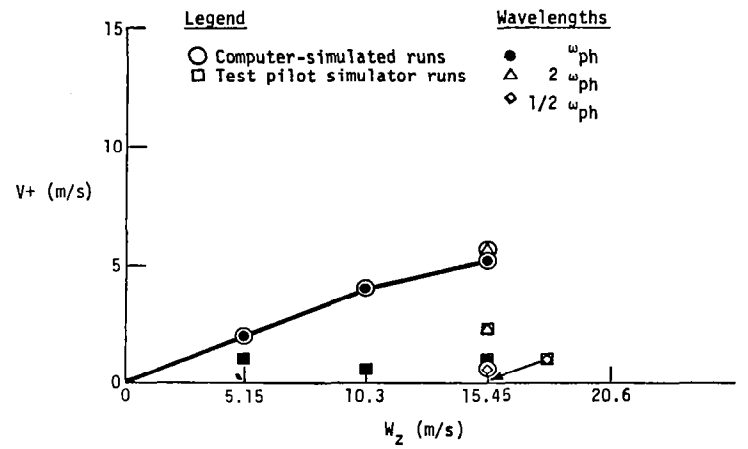

a) V+ values versus 1 - cosine wave amplitude and frequency.

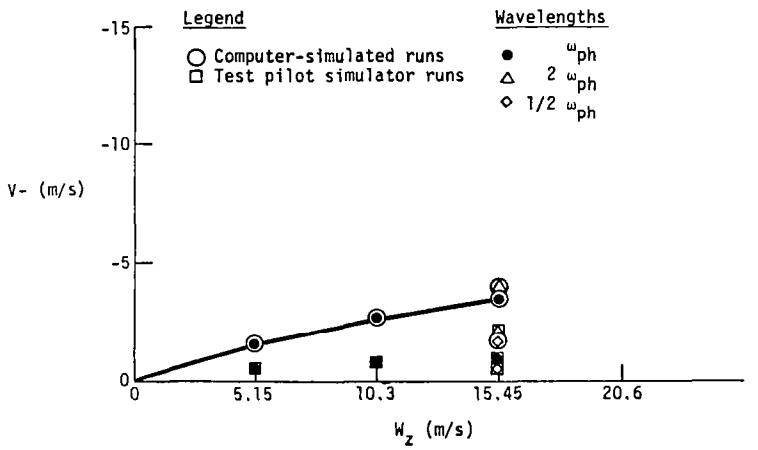

b) V- values versus 1 - cosine wave amplitude and frequency.

Figure 27 Airspeed deviation parameters for vertical 1 - cosine wave winds.

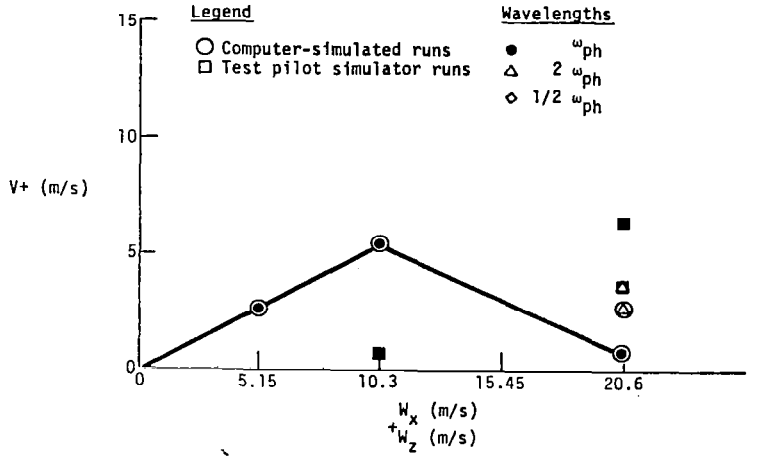

a) V+ values versus combination S-shape and 1 - cosine wave amplitude and frequency.

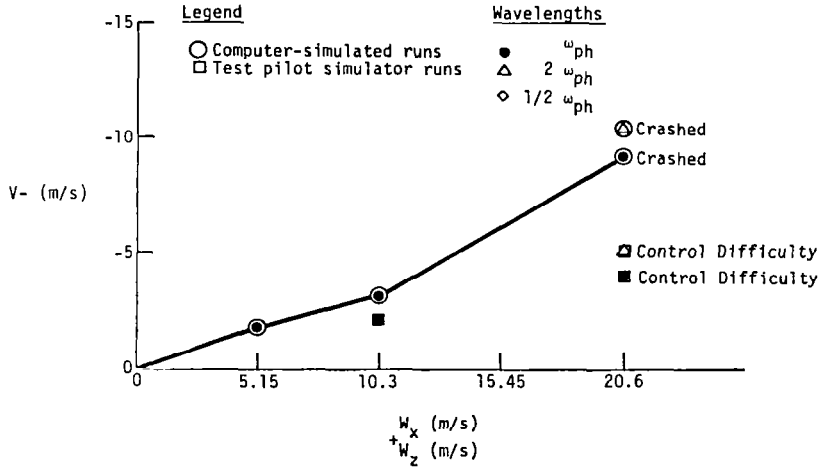

b) V- values versus combination S-shape and 1 - cosine wave amplitude and frequency.

Figure 28 Airspeed deviation parameters for combination longitudinal S-shape and vertical 1 - cosine wave winds.

CHAPTER 6. CONCLUDING REMARKS

The feasibility of a system for warning and detection of longitudinal wind shear has been discussed. The aircraft trajectory program, pilot control models, and the flight path deterioration parameters have also been discussed. The results of the computer and simulator runs through the longitudinal S-shape waves and sine waves indicate a need for further studies to examine the effects of large longitudinal wind gradients due to large amplitude waves at short wavelengths. A parametric analysis of a broader range of wave frequencies must be carried out to determine the bandwidth which is most hazardous to aircraft operations.

Control difficulties were noted with 1 - cosine downbursts, particularly the long duration wave at large amplitude and the strong downbursts combined with longitudinal shear. The authors believe that the combination longitudinal S-shape and vertical 1 - cosine wind profile is the most realistic model of a downburst cell wind field in the vicinity of the ground. Therefore, additional simulator studies should be carried out to study the response of the aircraft/pilot system to a wider range of combination downbursts and longitudinal shear waves.

The authors believe that the Doppler radar is the optimum wind measurement device for a wind shear detection system which provides the aircraft with advanced warning of hazardous shear conditions. As mentioned above, a downburst cell wind profile consists of a vertical 1 - cosine wave component and a longitudinal S-shape wave component. Because of the interrelationship of the longitudinal and vertical winds, it is probable that the measurement of only the longitudinal wind component along the flight path and the detection of longitudinal shear waves may provide a sufficient warning when a downburst hazard exists.

The present computer model has the capability to simulate pilots of varying skill. Further studies can be performed on "fine tuning" the

pilot model to simulate the best, average, or worst pilot. A simulator study of pilot elevator and thrust inputs in flight through wind gradients of varying magnitudes would yield necessary data for use in the simplified numerical model. It is also possible to put in the actual autopilot used in the aircraft to serve as the baseline pilot. The autopilot characteristics could easily be entered into the control logic in the aircraft trajectory model and used as the standard pilot for the wind shear warning and detection system.

In addition, the aircraft trajectory model used in the actual warning system would require a more accurate but equally simplified model of engine response to pilot throttle input. The most accurate and concise aerodynamic data for commercial transports must also be available for improved accuracy of the warning system aircraft trajectory software.

Finally, the issue of how flight path deterioration should be quantitatively determined and presented as a go/no-go signal to the pilot or air traffic controller must be resolved. The results of the computer study shows that while the altitude deviation parameters can be misleading (except possibly for downburst warnings), the airspeed deviation parameters may yield useful results when longitudinal disturbances are present. The authors believe that V- may be a useful warning parameter because it reveals information about how far below V_{ref} an aircraft may deviate. An example of the usefulness of V- as a warning parameter is given by the two severe combination S-shape and downburst waves which took the test pilot by surprise, causing serious control difficulty. The large values of V- would have warned the pilot that the aircraft airspeed would deviate significantly below V_{ref} and into the stall region. This would indicate a no-go situation and the warning system would have alerted the aircraft before entering the Doppler-monitored flight path. Further tests are needed to determine the go/no-go decision value. It is also possible to use the minimum airspeed obtained during the simulated trajectory as a quantitative deterioration parameter. If this value was below the go/no-go decision value (some value around the stall speed) the aircraft would be forewarned of the hazardous conditions existing along its anticipated flight path.

REFERENCES

1. National Transportation Safety Board. "Eastern Airlines, Inc., Boeing 727-225, John F. Kennedy International Airport, Jamaica, New York, June 24, 1975," Aircraft Accident Report No. NTSB-AAR-76-8, National Transportation Safety Board, Washington, D. C., March 12, 1976.

2. Fujita, T. T., and F. Caracena. "An Analysis of Three Weather-Related Aircraft Accidents," Bulletin of the American Meteorological Society, Vol. 58, No. 11, November, 1977.

3. McCarthy, J., E. F. Blick, and R. R. Bensch. "Jet Transport Performance in Thunderstorm Wind Shear Conditions," NASA CR 3207, December, 1979.

4. Frost, W., and W. A. Crosby. "Investigations of Simulated Aircraft Flight through Thunderstorm Outflows," NASA CR 3052, September, 1978.

5. Frost, W., and K. R. Reddy. "Investigations of Aircraft Landing in Variable Wind Fields," NASA CR 3073, December, 1978.

6. Turkel, B. S., and W. Frost. "Pilot-Aircraft System Response to Wind Shear," NASA CR 3342, November, 1980.

7. Tinsley, H. G., F. G. Coons, and L. Wood. "Possible Near-Term Solutions to the Windshear Hazard," Proceedings of the United States Air Force Low Level Windshear Conference, Travis AFB, California, May 3-4, 1978, p. 2:1-18.

8. Bedard, A. J., W. H. Hooke, and D. W. Beran. "The Dulles Airport Pressure-Jump Detector Array for Gust Front Detection," Bulletin of the American Meteorological Society, pp. 920-926, September, 1977.

9. McCarthy, J., E. F. Blick, and K. L. Elmore. "An Airport Wind Shear Detection and Warning System Using Doppler Radar--A Feasibility Study," NASA CR 3379, January, 1981.

10. Etkin, B. Dynamics of Atmospheric Flight. New York: John Wiley & Sons, Inc., 1972.

11. Davies, D. P. Handling the Big Jets. London: Civil Aviation Authority, 1973.

12. Smith, V. K. Private communication. Arnold Engineering and Development Center, Tullahoma, Tennessee, November, 1980.

APPENDICES

APPENDIX A

LANDING CHARACTERISTICS OF A B727 CLASS MEDIUM-SIZED JET TRANSPORT*

Flaps 30°
Gear Down
Glide Slope Angle -3.0°

V	trim airspeed, 70.0 m/s
m	aircraft mass, 63,958.0 kg
I_{yy}	moment of inertia, 6.1×10^6 kg - m^2
$\bar{c}$	mean chord length, 4.57 m
A	wing area, 145.0 m^2
C_{L_o}	0.74
C_{L_α}	6.99/rad
$C_{L_{\delta_E}}$	0.361/rad
C_{L_q}	10.0/rad
$C_{L_{\dot{\alpha}}}$	-7.6/rad
C_{D_o}	0.152
C_{D_α}	0.3/rad
$C_{D_{\alpha^2}}$	2.4/rad^2
$C_{D_{\delta_E}}$	0.0/rad
C_{m_o}	-0.25
C_{m_α}	-1.40/rad
$C_{m_{\delta_E}}$	-1.59/rad
C_{m_q}	-30.0/rad
$C_{m_{\dot{\alpha}}}$	-2.16/rad

*Aerodynamic data used in an airline flight simulator.

APPENDIX B

SAMPLE CALCULATION OF FLIGHT PATH DETERIORATION PARAMETERS

The flight path deterioration parameters (FPDP) quantitatively describe the aircraft trajectory by glide slope deviations and airspeed deviations from reference airspeed. Normalized altitude, HP/HG, was chosen as the FPDP representing glide slope deviation, where HP is the height of the aircraft above the ground and HG is the height of the glide slope above the ground. This formulation was chosen over root mean square calculations of glide slope deviation ($\Delta H = HP - HG$) because it accounts for the fact that altitude deviations become more serious at lower altitudes than at higher altitudes.

The airspeed deviation parameter chosen was simply the deviation of airspeed from the reference value ($\Delta V = V - V_{ref}$). In both glide slope and airspeed deviation parameters, the positive deviations are examined separately from the negative deviations to avoid the cancellation errors.

Figure B.1 shows a hypothetical aircraft trajectory of which a quantitative analysis of glide slope and airspeed deviation is desired. The values of airspeed and altitude for each point on the trajectory is given in Table B.1. Also given in Table B.1 are the FPDP's, airspeed deviation from reference airspeed, and normalized altitude. Using the data from Table B.1, the FPDP's are calculated as follows:

Computation of V+

Total points airspeed is above or at V_{ref} = 15 = j

$$V+ = \frac{1}{j} \sum_{i=1}^{j} (V_i - V_{ref}) = \frac{1}{15} \left(\begin{array}{l} 0.0 + 1.0 + 2.0 + 4.0 + 5.0 + 6.0 + 4.0 \\ + 1.0 + 0.0 + 1.0 + 2.0 + 3.0 + 1.0 \\ + 0.0 + 0.0 \end{array} \right)$$

$$\frac{1}{15} [30.0 \text{ m/s}] = \boxed{2.0 \text{ m/s}} \text{ (average airspeed deviation above } V_{ref} = +2.0 \text{ m/s)}$$

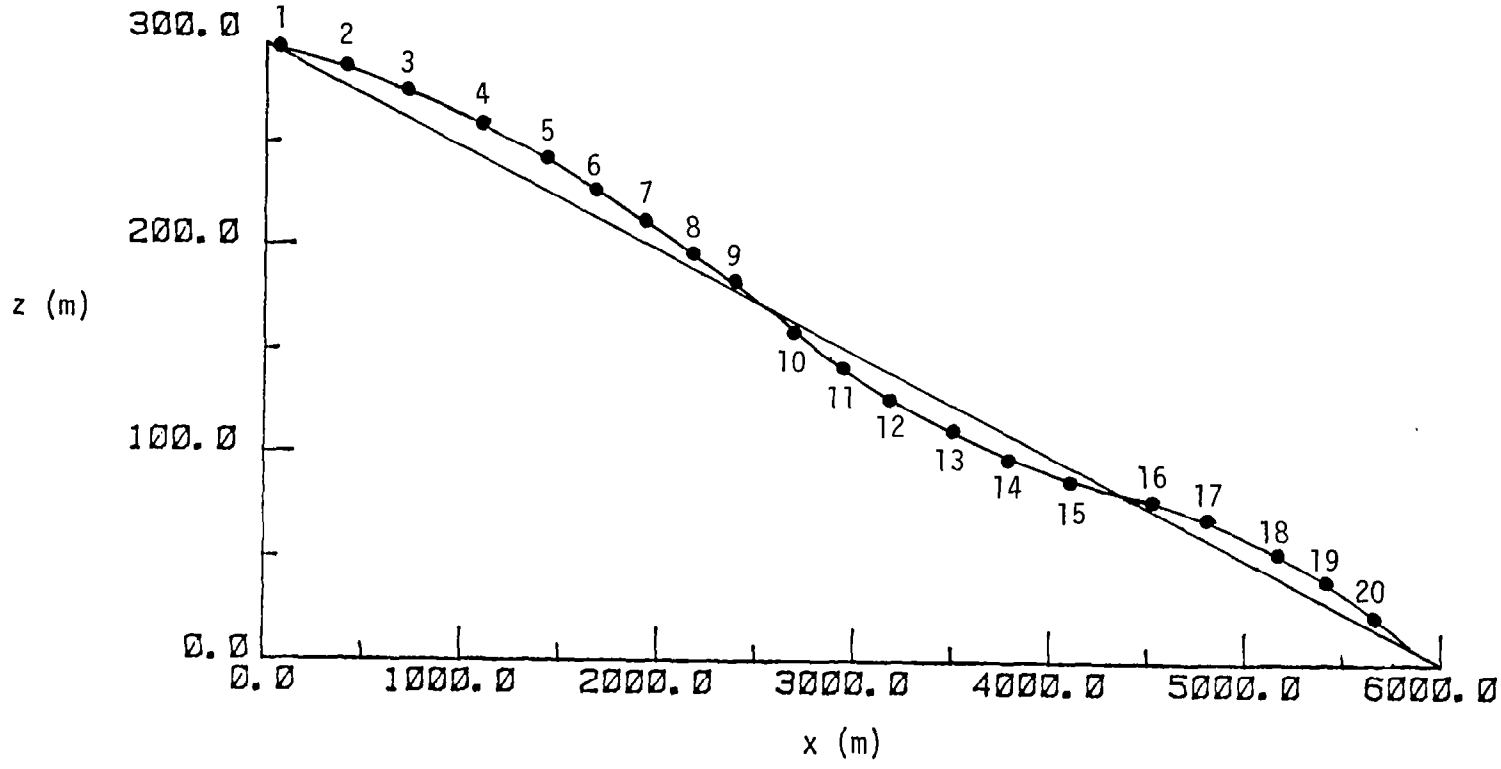

Figure B.1 Hypothetical aircraft trajectory.

TABLE B.1 Hypothetical Aircraft Trajectory Data.

Point	Airspeed V (m/s)	Reference Airspeed V_{ref} (m/s)	Airspeed Deviation $V-V_{ref}$ (m/s)	Airspeed Above or At V_{ref}	Airspeed Below V_{ref}	Aircraft Height Above Ground HP (m)	Glide Slope Height Above Ground HG (m)	Normalized Altitude HP/HG (nondimensional)	Above or On Glide Slope	Below Glide Slope
1	70.0	70.0	0.0	✓		300.0	300.0	1.00	✓	
2	71.0	70.0	1.0	✓		295.0	280.0	1.05	✓	
3	72.0	70.0	2.0	✓		280.0	265.0	1.06	✓	
4	74.0	70.0	4.0	✓		265.0	245.0	1.08	✓	
5	75.0	70.0	5.0	✓		245.0	230.0	1.07	✓	
6	76.0	70.0	6.0	✓		230.0	220.0	1.05	✓	
7	74.0	70.0	4.0	✓		215.0	205.0	1.05	✓	
8	71.0	70.0	1.0	✓		200.0	195.0	1.03	✓	
9	69.0	70.0	-1.0		✓	180.0	180.0	1.00	✓	
10	68.0	70.0	-2.0		✓	160.0	165.0	0.97		✓
11	67.0	70.0	-3.0		✓	140.0	150.0	0.93		✓
12	69.0	70.0	-1.0		✓	120.0	140.0	0.86		✓
13	70.0	70.0	0.0	✓		105.0	125.0	0.84		✓
14	71.0	70.0	1.0	✓		90.0	105.0	0.86		✓
15	72.0	70.0	2.0	✓		80.0	90.0	0.89		✓
16	73.0	70.0	3.0	✓		75.0	70.0	1.07	✓	
17	71.0	70.0	1.0	✓		60.0	50.0	1.20	✓	
18	70.0	70.0	0.0	✓		50.0	35.0	1.43	✓	
19	70.0	70.0	0.0	✓		30.0	25.0	1.20	✓	
20	69.0	70.0	-1.0		✓	15.0	10.0	1.50	✓	
Total 20				15	5				14	6

Computation of V-

Total points airspeed is below V_{ref} = 5 = k

$$V- = \frac{1}{k} \sum_{i=1}^{k} (V_i - V_{ref}) = \frac{1}{5} \left((-1.0) + (-2.0) + (-3.0) + (-1.0) + (-1.0) \right)$$

$\frac{1}{5}$ [-8.0 m/s] = $\boxed{-1.6 \text{ m/s}}$ (average airspeed deviation below V_{ref} = -1.6 m/s)

Computation of GS+

Total points aircraft is above or on glide slope = 14 = n

$$GS+ = \frac{1}{n} \sum_{i=1}^{n} \frac{HP_i}{HG_i} = \frac{1}{14} \left(\begin{array}{l} 1.00 + 1.05 + 1.06 + 1.08 + 1.07 + 1.05 + 1.05 \\ \quad + 1.03 + 1.00 + 1.07 + 1.20 + 1.43 + 1.20 \\ \quad + 1.50 \end{array} \right)$$

$\frac{1}{14}$ [15.79] = $\boxed{1.13}$ (average displacement of aircraft above glide slope = 13 percent above glide slope height)

Computation of GS-

Total points aircraft is below glide slope = 6 = m

$$GS- = \frac{1}{m} \sum_{i=1}^{m} \frac{HP_i}{HG_i} = \frac{1}{6} \left(0.97 + 0.93 + 0.86 + 0.84 + 0.86 + 0.89 \right) = \boxed{0.89}$$

(average displacement of aircraft below glide slope = 11 percent below glide slope height)

1. REPORT NO.	2. GOVERNMENT ACCESSION NO.	3. RECIPIENT'S CATALOG NO.
NASA CR-3480		

4. TITLE AND SUBTITLE	5. REPORT DATE
FEASIBILITY STUDY OF A PROCEDURE TO DETECT AND WARN OF LOW-LEVEL WIND SHEAR	November 1981
	6. PERFORMING ORGANIZATION CODE
7. AUTHOR(S) Barry S. Turkel, Philip A. Kessel, and Walter Frost	8. PERFORMING ORGANIZATION REPORT #
9. PERFORMING ORGANIZATION NAME AND ADDRESS	10. WORK UNIT NO. M-365
FWG Associates, Inc. R.R. 2, Box 271-A Tullahoma, Tennessee 37388	11. CONTRACT OR GRANT NO. NAS8-33458
	13. TYPE OF REPORT & PERIOD COVERED Contractor Report
12. SPONSORING AGENCY NAME AND ADDRESS National Aeronautics and Space Administration Washington, D.C. 20546	14. SPONSORING AGENCY CODE

15. SUPPLEMENTARY NOTES

Marshall Technical Monitor: Dennis W. Camp
Final Report

16. ABSTRACT

The feasibility of a proposed Doppler radar system for providing an aircraft with advanced warning of longitudinal wind shear is described. This system uses a Doppler radar beamed along the glide slope linked with an on-line microprocessor containing a two-dimensional, three-degree-of-freedom model of the motion of an aircraft including pilot/autopilot control. The Doppler-measured longitudinal glide slope winds are entered into the aircraft motion model, and a simulated controlled aircraft trajectory is calculated. Several flight path deterioration parameters (FPDP) are calculated from the computed aircraft trajectory information. These parameters quantify the airspeed and flight path deviation of the computed trajectory from the optimum trajectory and are intended to be used by the pilot or air traffic controller to decide whether the projected flight path is safe or unsafe. This report discusses the aircraft trajectory program, pilot control models, and the flight path deterioration parameters. Comparisons are presented between the performance of the computer model and a test pilot in a NASA Ames flight simulator through longitudinal and vertical wind fields characteristic of a thunderstorm wind field.

17. KEY WORDS	18. DISTRIBUTION STATEMENT
Wind Shear Turbulence Low-Level Wind Flow Aviation Safety	Unclassified - Unlimited Subject Category 47

19. SECURITY CLASSIF. (of this report)	20. SECURITY CLASSIF. (of this page)	21. NO. OF PAGES	22. PRICE
Unclassified	Unclassified	81	A05

For sale by National Technical Information Service, Springfield, Virginia 22161

NASA-Langley, 1981